Influences on rainfall anomalies over eastern China and CNRM-CM5 projected changes of the boreal summer intraseasonal oscillations (BSISOs)

Jiangyu Mao, Jianying Li, and Guoxiong Wu

Institute of Amospheric Physics, Beijing

2017. 08. 01 ICTP

Outline

1. **Overview**

2. **Influences of BSISOs on rainfall anomalies over eastern China**

3. **Future changes of 30–60-day BSISO projected by CNRM-CM5 model**

4. **Summary**

Discovery of the eastward-propagating 40-50-day intraseasonal oscillation (MJO) in tropical atmosphere during boreal winter

Madden and Julian (1971, 1972)

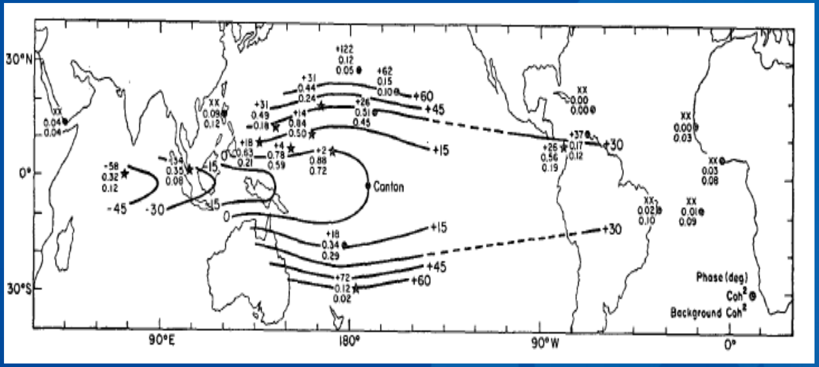

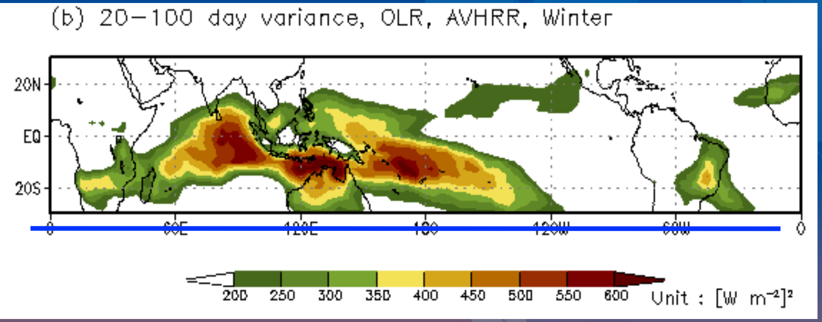

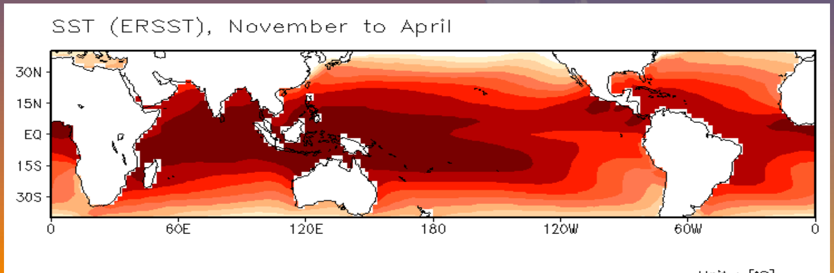

Waliser et al.(2009)

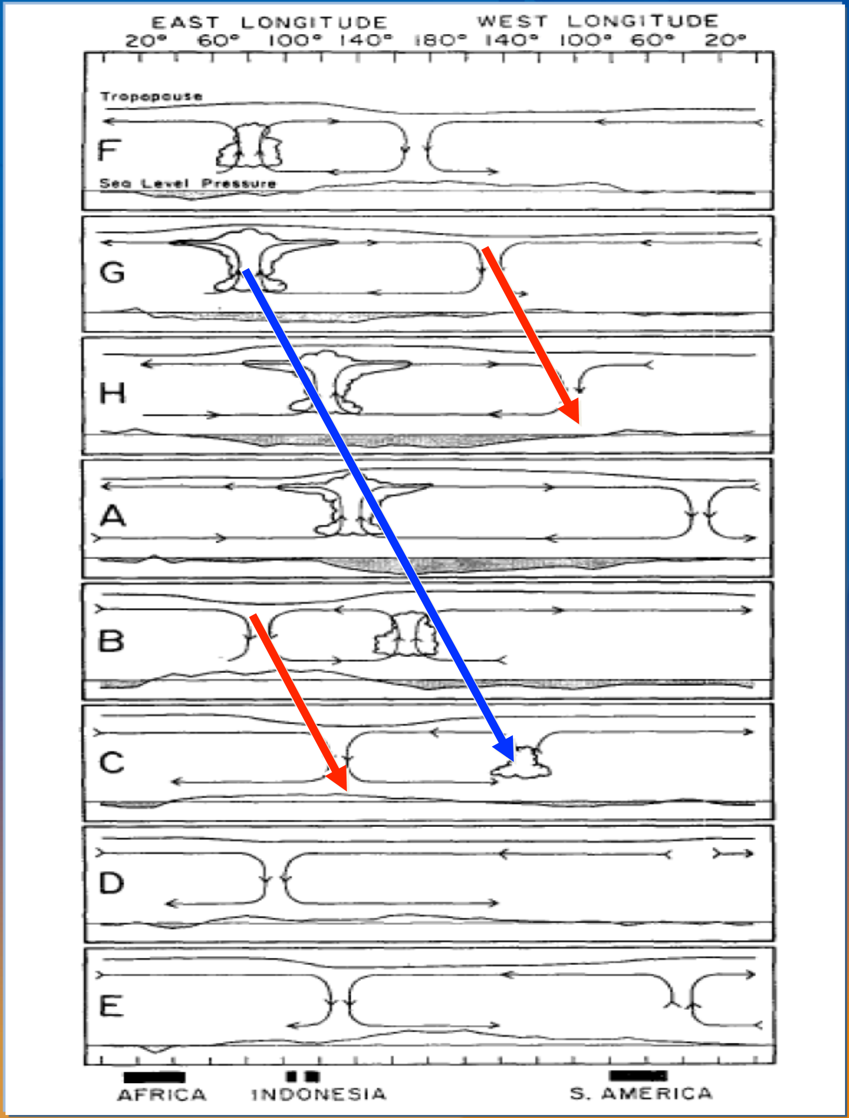

Global Impacts of MJO on Weather and Climate

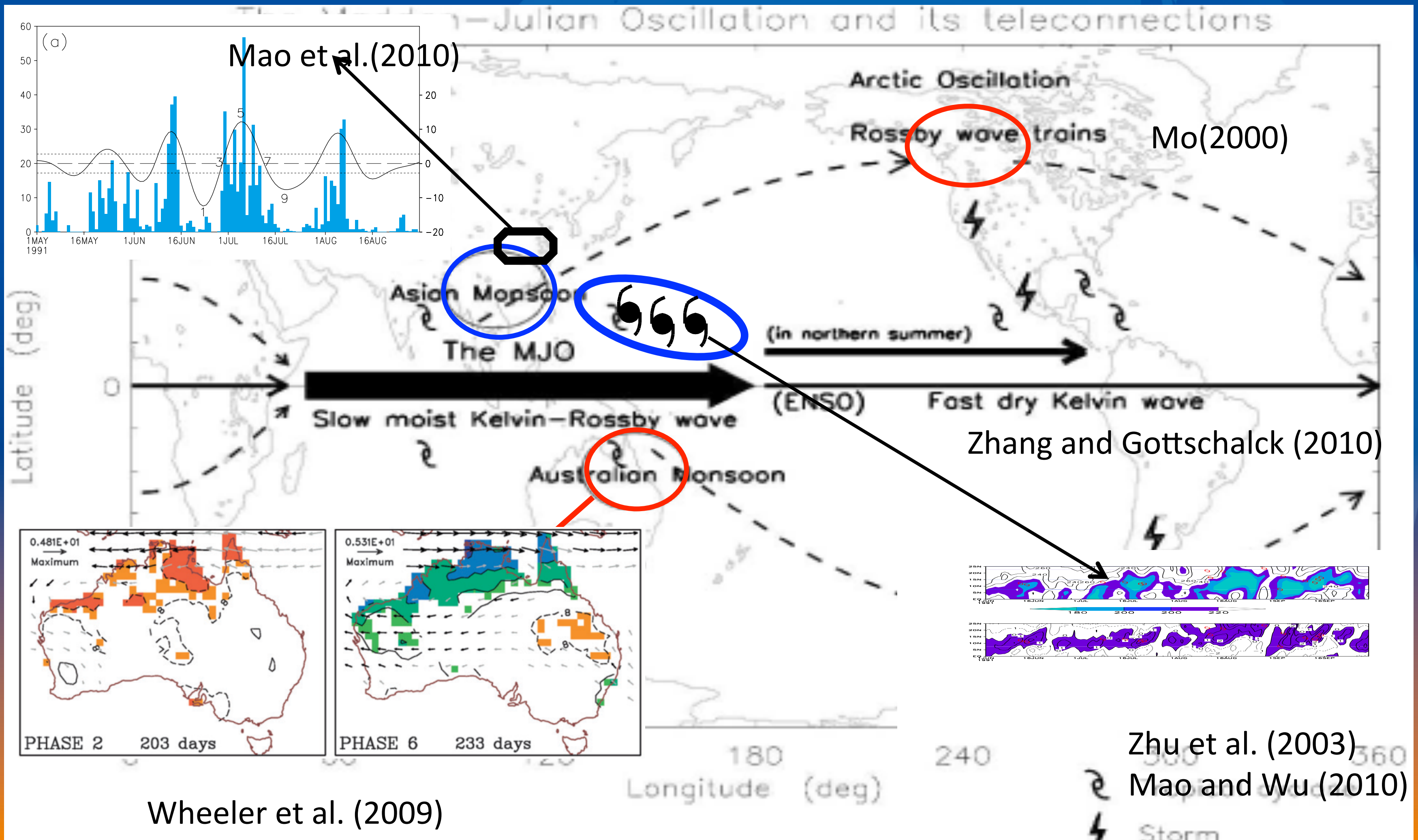

Lin et al. (2006)

Progresses in MJO *Monitoring, simulation diagnostics, and Forecast*

- ◆**Developing Real-time Multivariate MJO (RMM) index (Wheeler and Hendon, 2004)**
- ◆**Applying MJO diagnostics to Climate models for operational forecast**

(1) Real-time MJO Index

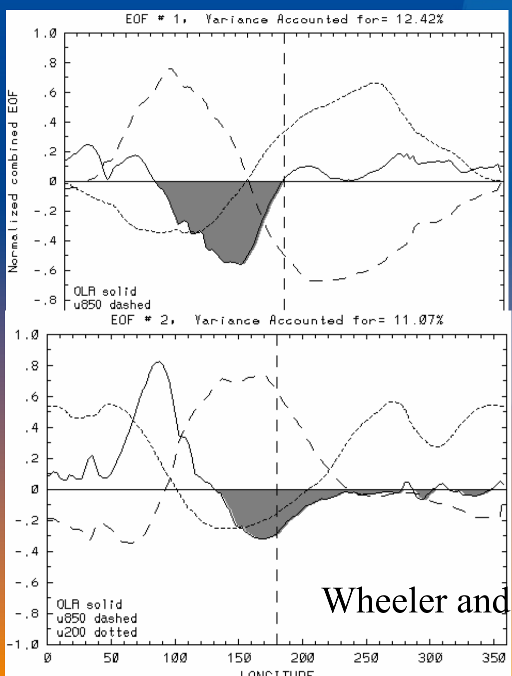

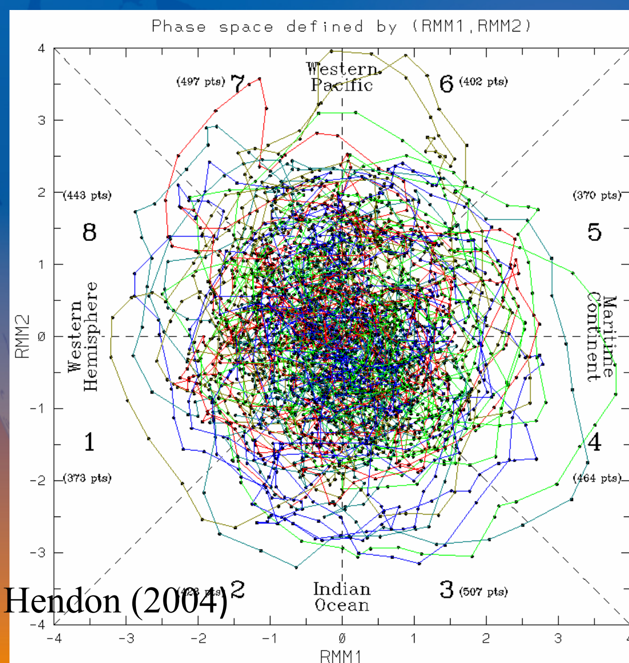

Wheeler and Hendon (2004)

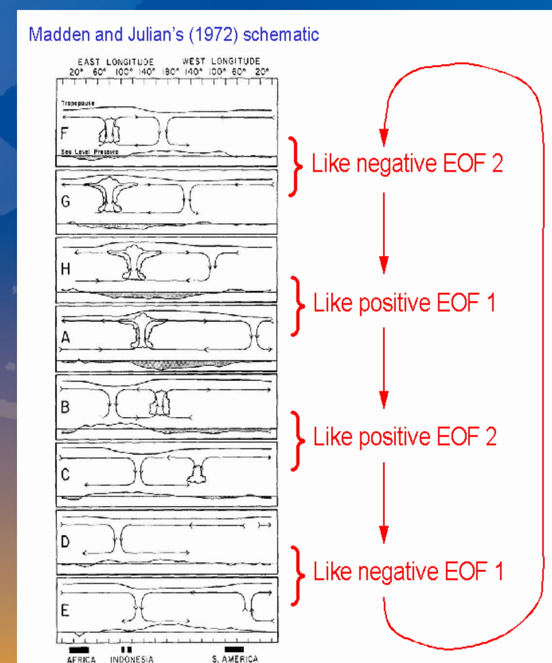

Phase-space representation of MJO

Rainfall probabilities for eight MJO phases (Wheeler et al. 2009)

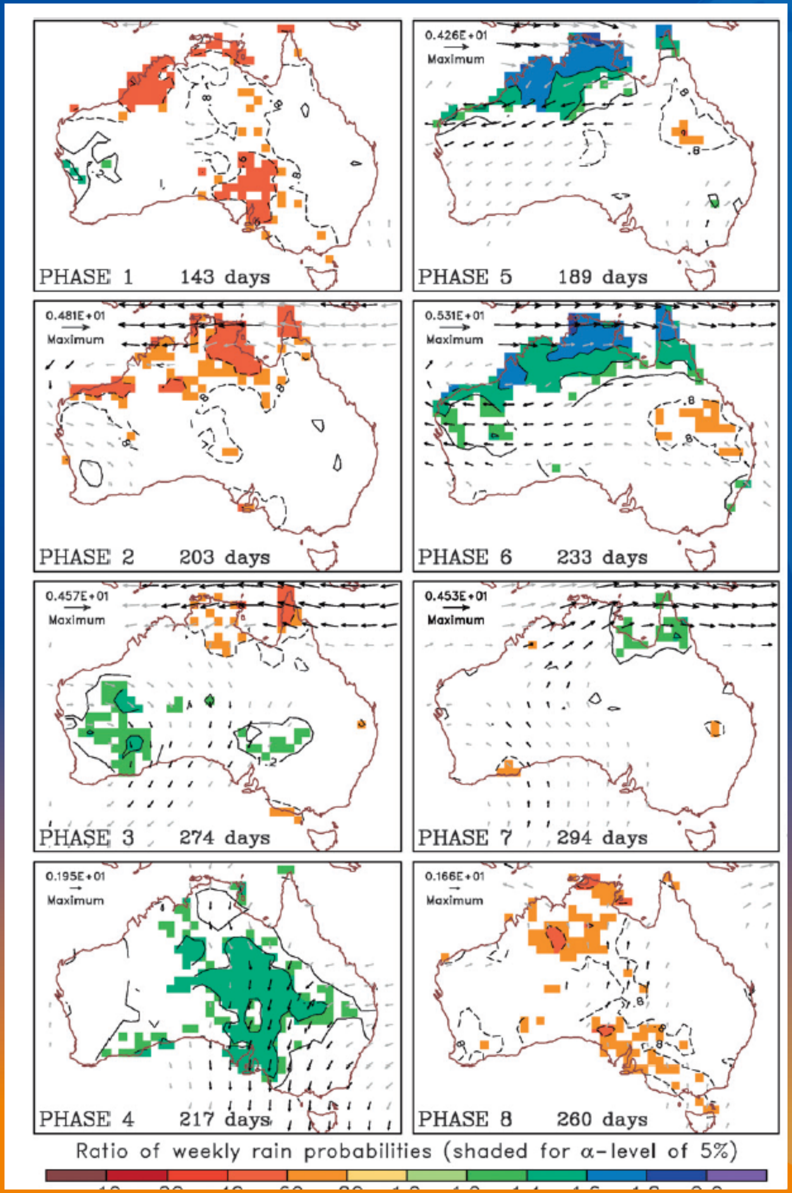

CPC: MJO monitoring and operational intraseasonal forecast

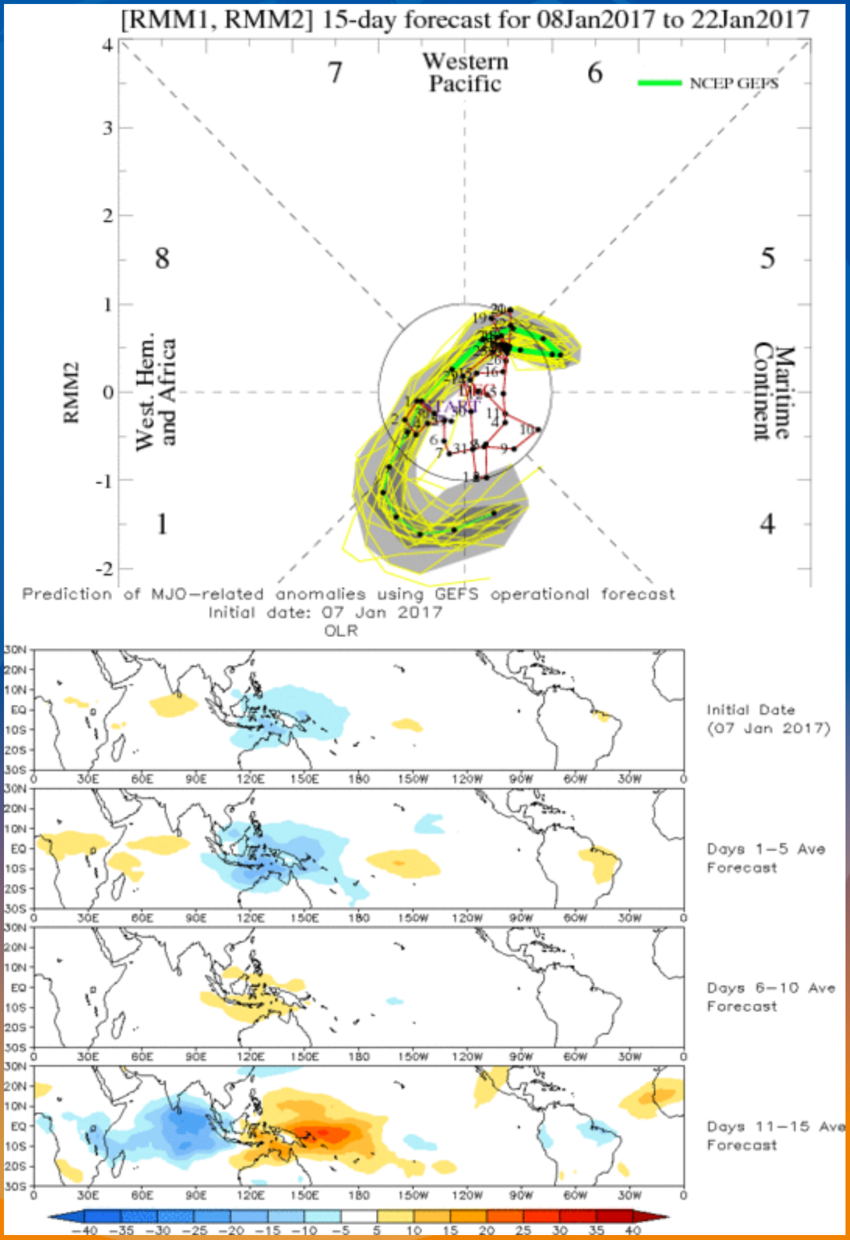

Progresses in MJO Monitoring, simulation diagnostics, and Forecast

◆**MJO seasonality (developing Real-time Boreal summer intraseasonal oscillation (BSISO) indices (Lee et al. 2013) to reflect *northward* propagation of BSISOs)**

◆ **Applying BSISO diagnostics to Climate models for operational forecast (APEC climate Center)**

(2) Real-time BSISO Indices

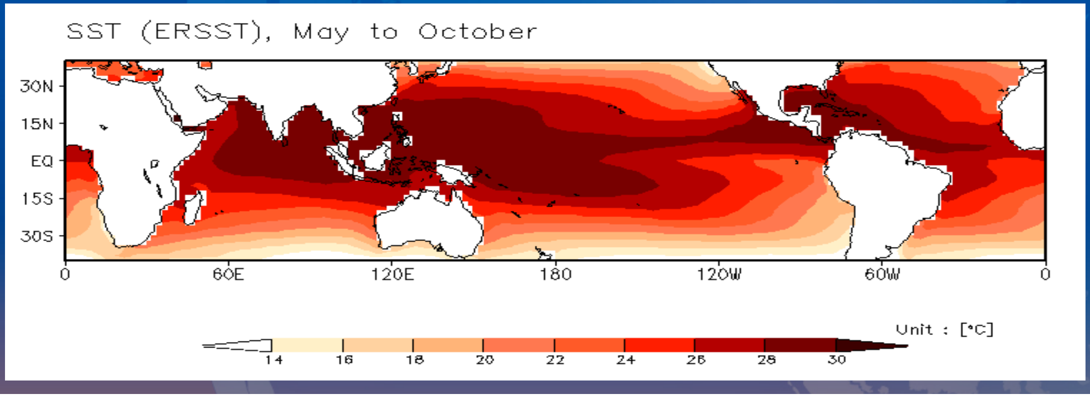

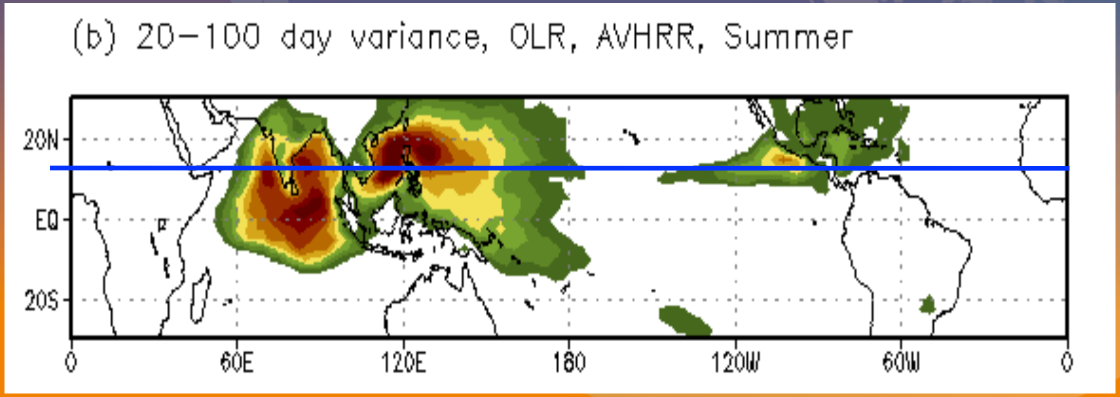

Real-time BSISO Indices (BSISO1 for 30-60 days and BSISO2 for 10-30 days)

Lee et al. (2013)

30–60-day

Canonical eastward-propagating ISO with northward-propagating component

10–30-day

Westward and northwestward propagating oscillation during pre-monsoon and monsoon-onset periods

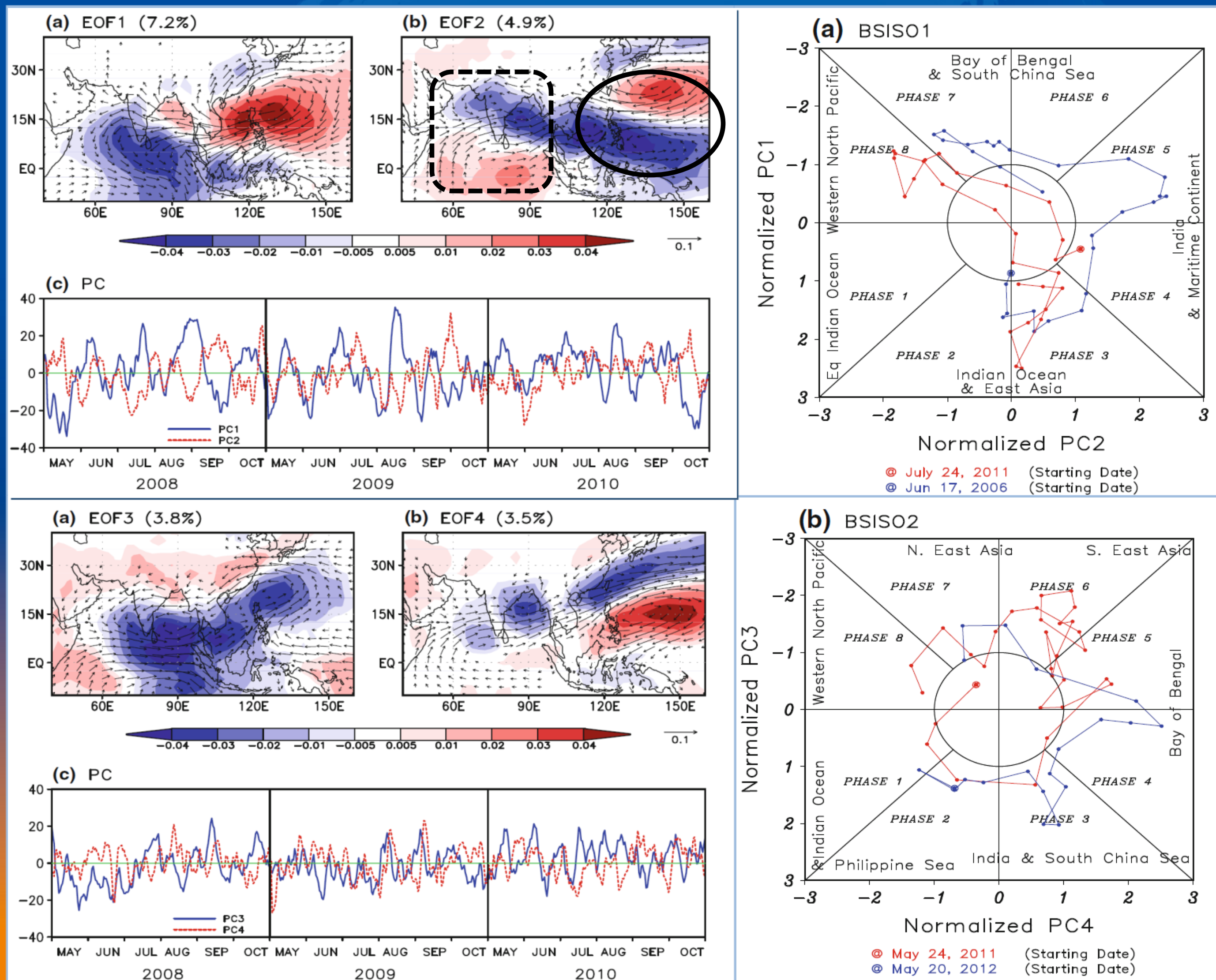

APCC: Operational Model BSISO Forecast

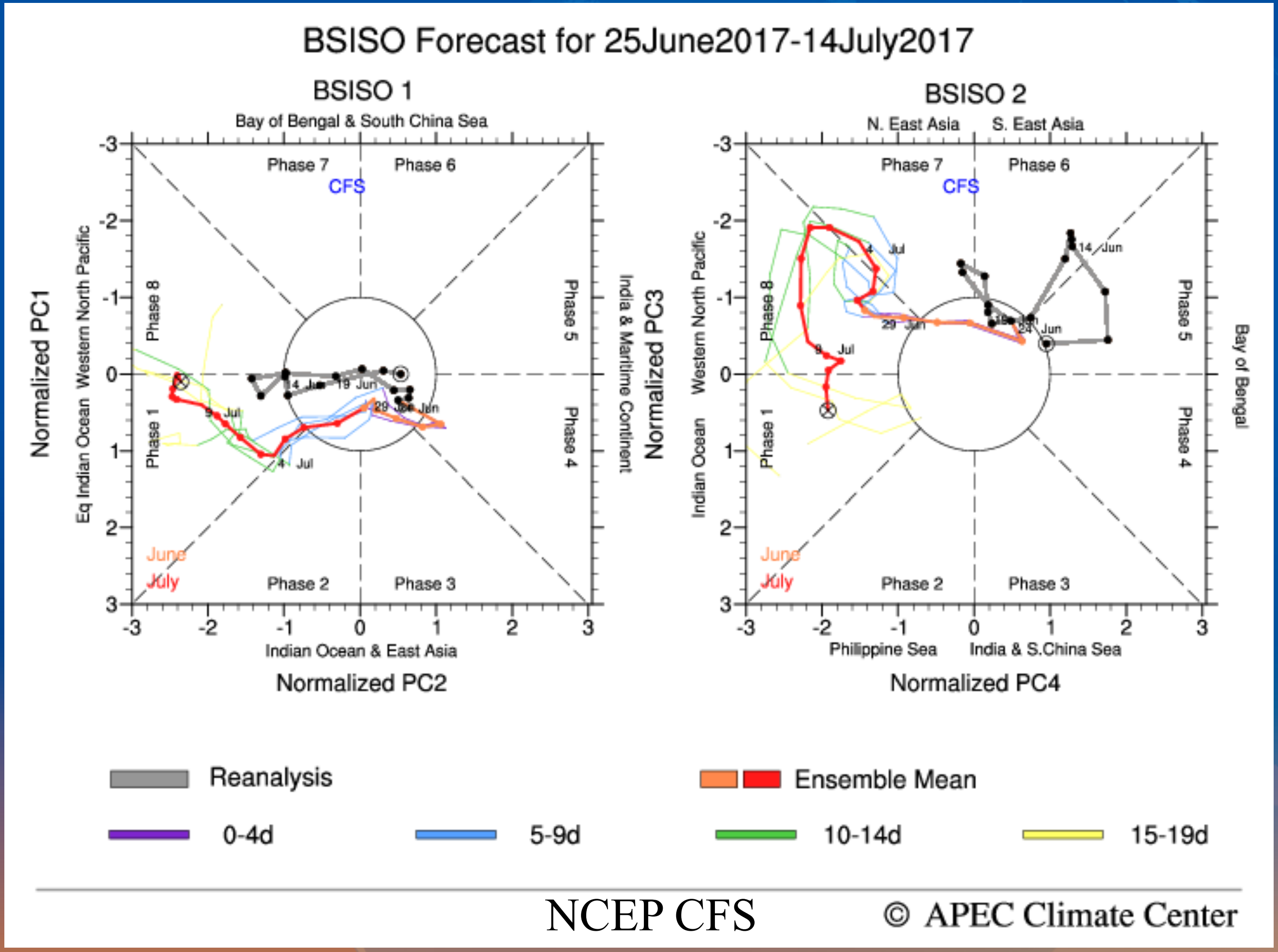

The BSISO forecast activity has been initiated in 2013 with the goal of improving our ability to understand and forecast the BSISO based on numerical models in cooperation with the CAS/WCRP Working Group on Numerical Experimentation (WGNE) Madden Julian Oscillation (MJO) Task Force, and hosted at the APEC Climate Center (APCC).

Outline

1. **Overview**
2. **Influences of BSISOs on rainfall anomalies over eastern China**
3. **Future changes of 30–60-day BSISO projected by CNRM-CM5 model**
4. **Summary**

Impacts of BSISOs on rainfall over eastern China (1981-2007)

1）30-60-day BSISO

Li et al. (2015, CD)

OLR (shading) and 850hPa wind anomalies

EOF1

EOF2

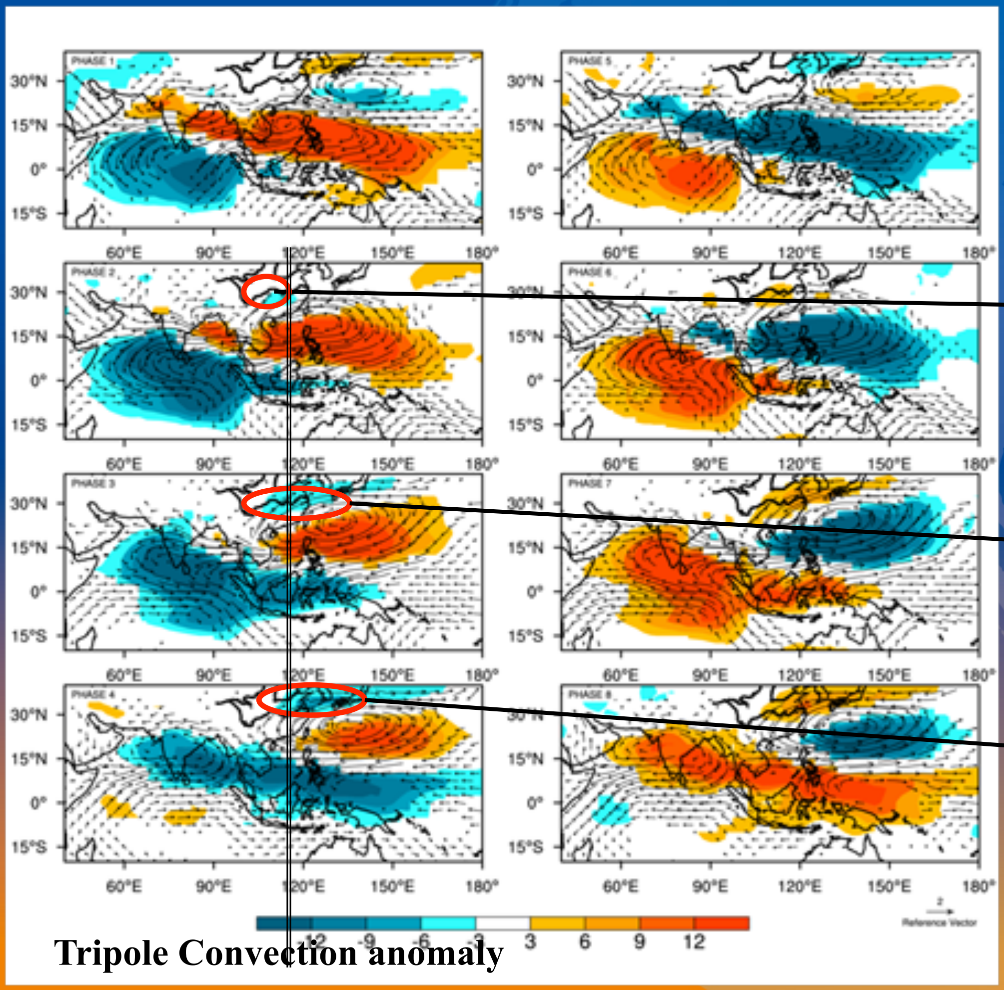

Station-Obs. Rainfall anomalies

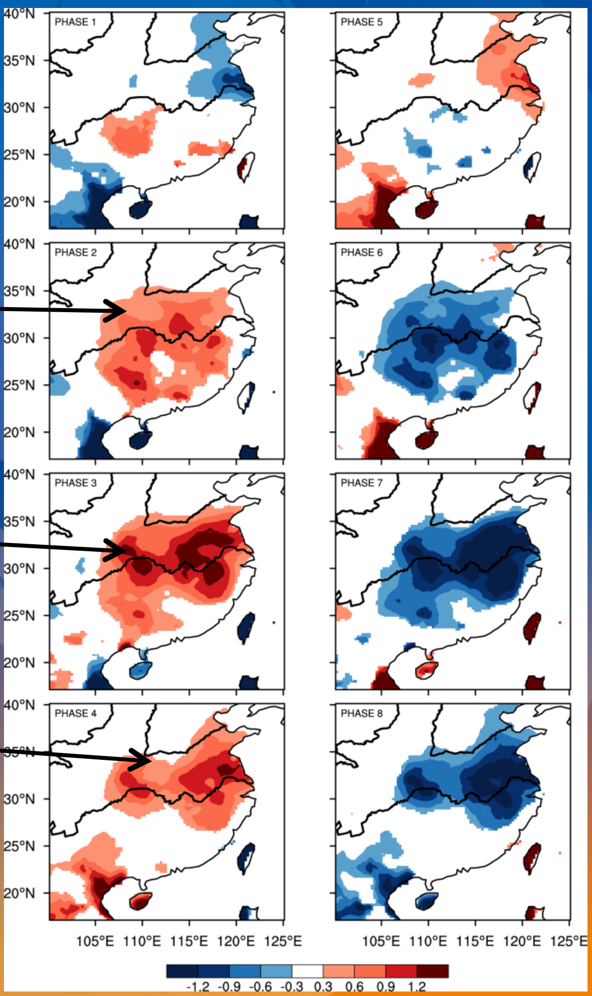

20-50-day ISO of Yangtze Rainfall（based on 1979-2003 datasets）

Mao et al. (2010, CD)

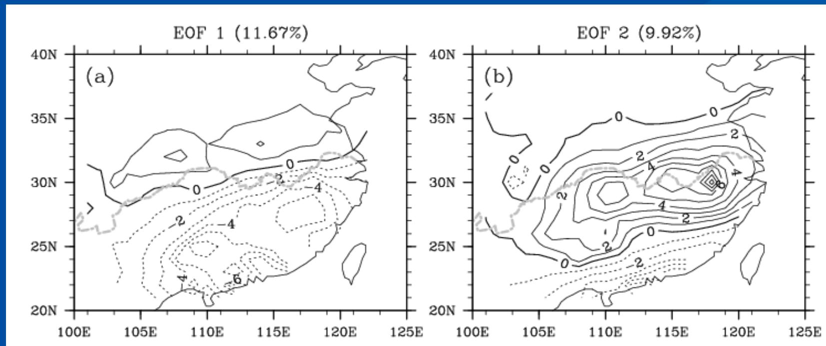

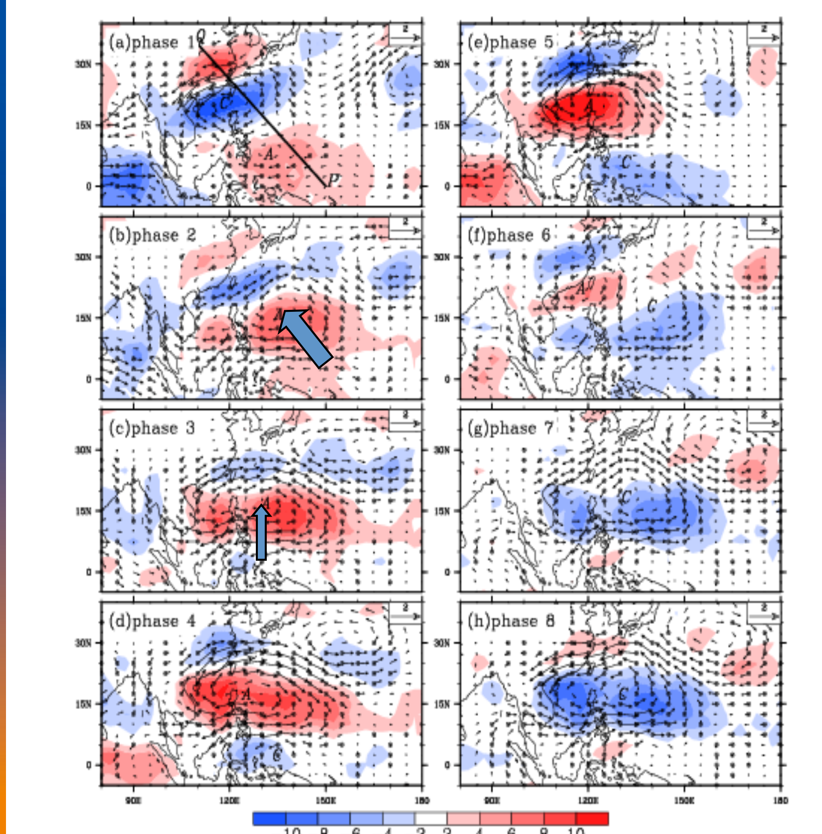

OLR (shading) and 850-hPa wind anomalies

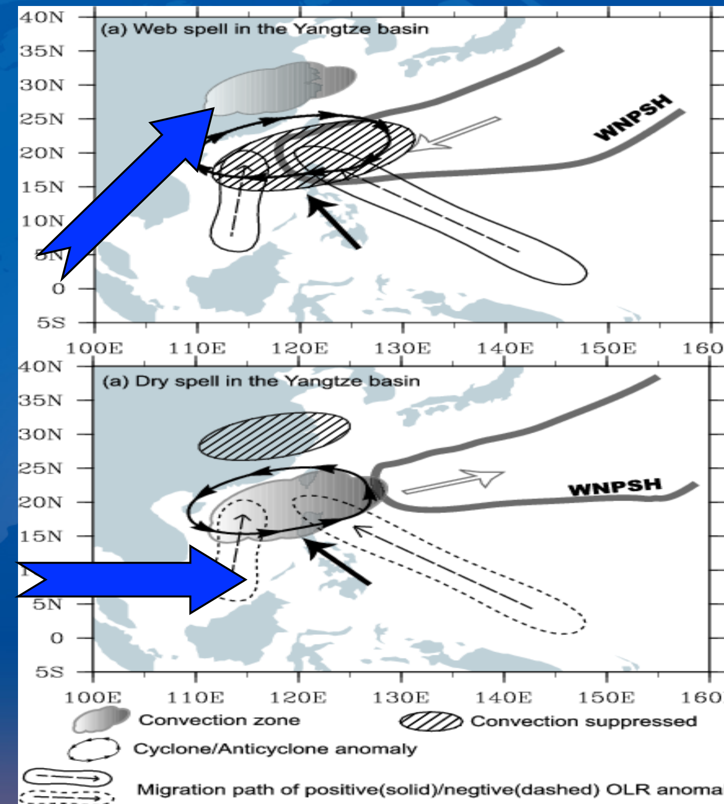

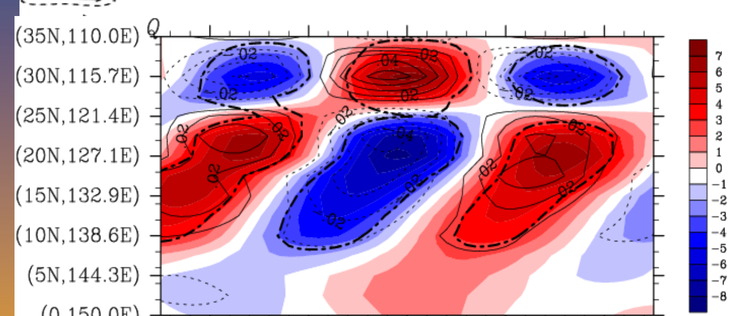

Lagged regression of OLR anomalies (W m-2) onto the 20-50 day ISO index of the Yangtze rainfall for day -25 to day 25 with a lag of 1 day along (a) line PQ

Impacts of BSISOs on rainfall over eastern China (1981-2007)

1） 30-60-day BSISO

Anomalous Divergence (shading) and vertical circulation along 115-120E

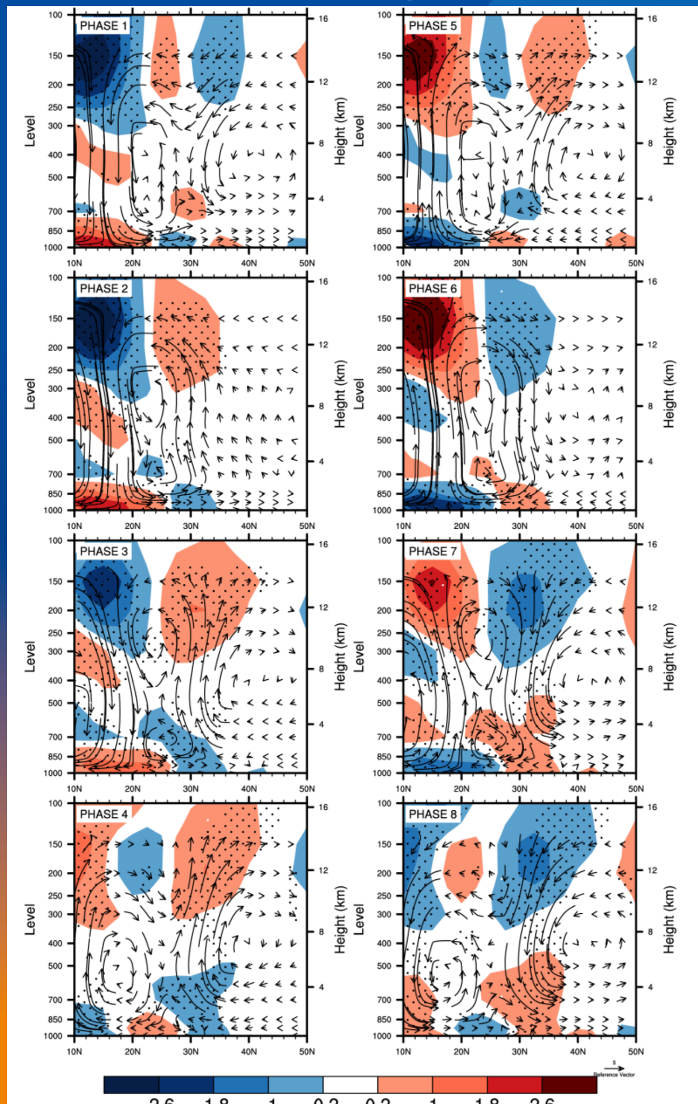

Anomalous ω (contour) and integrated precipitable water (300-1000 hPa)

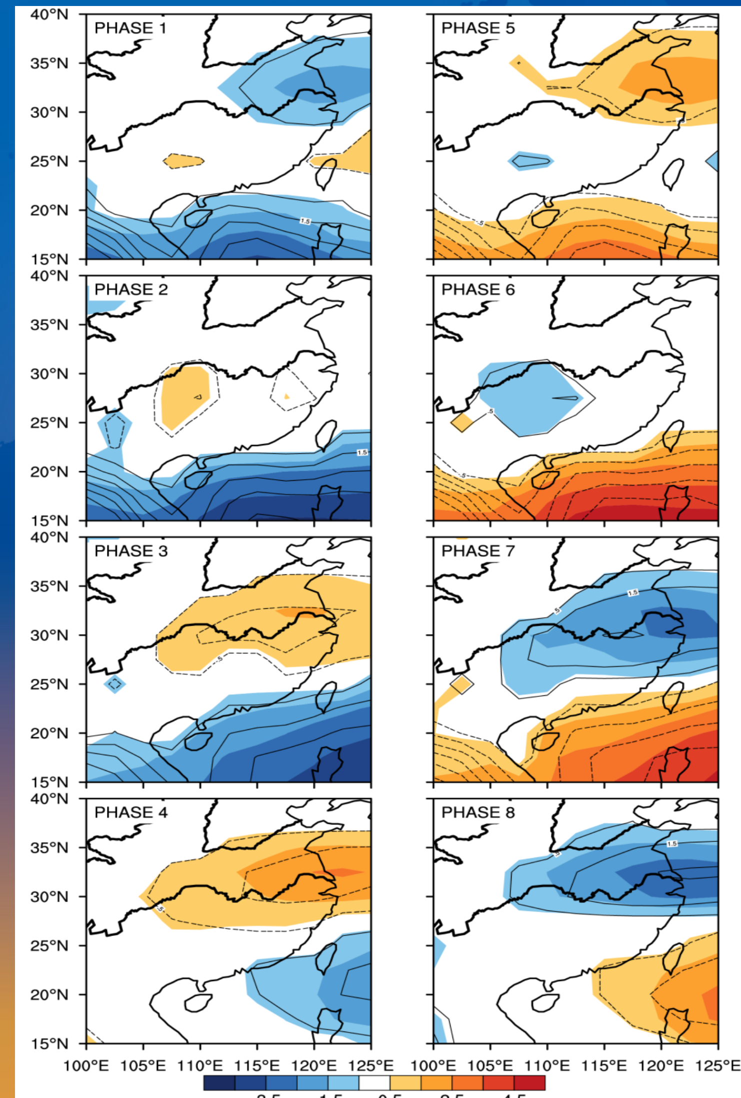

Impacts of BSISOs on rainfall over eastern China (1981-2007)

1）30-60-day BSISO

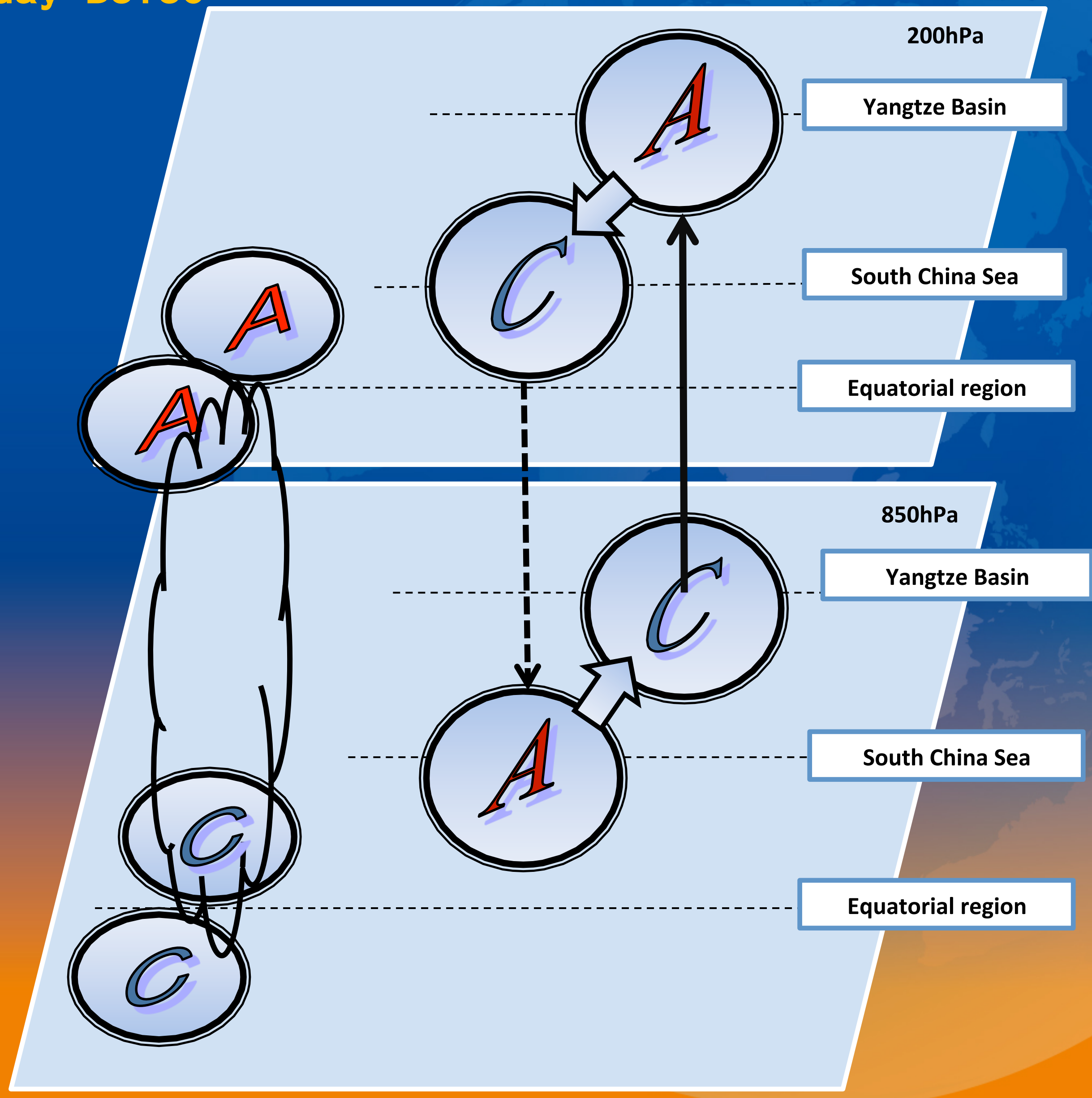

Impacts of BSISOs on rainfall over eastern China (1981-2007)

2) 10–30-day BSISO

Li et al. (2015, CD)

EOF3

EOF4

OLR (shading) and 850hPa wind anomalies

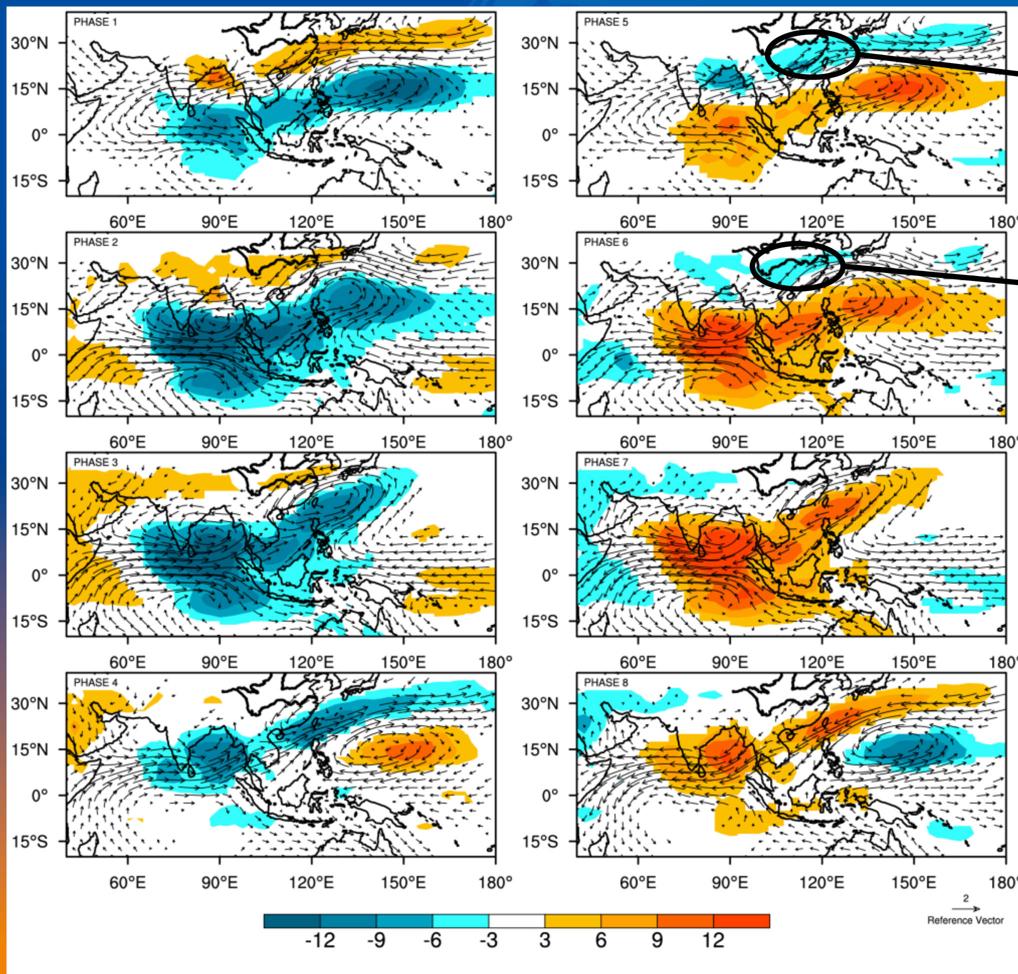

Station-Obs. Rainfall anomalies

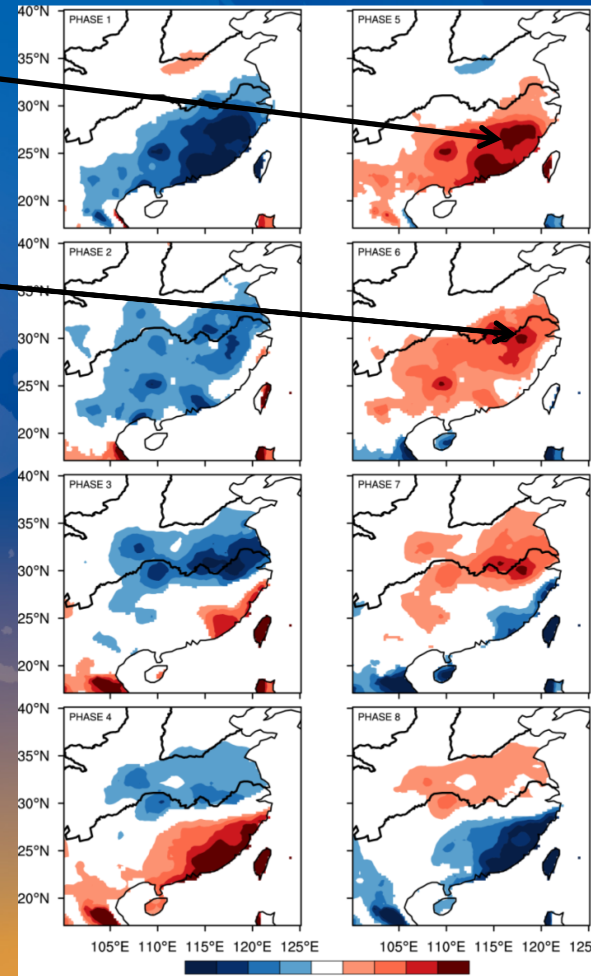

Impacts of BSISOs on rainfall over eastern China (1981-2007)

2) 10-30-day BSISO

Anomalous Divergence

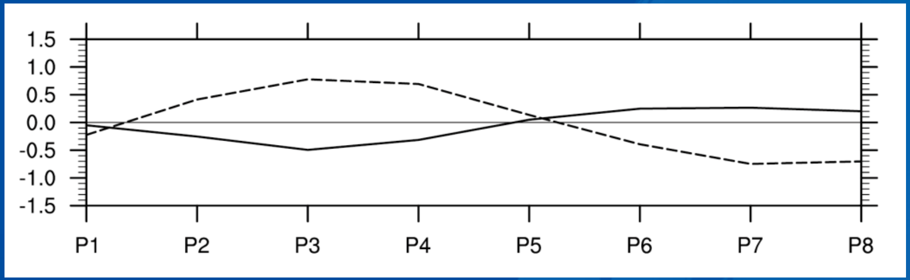

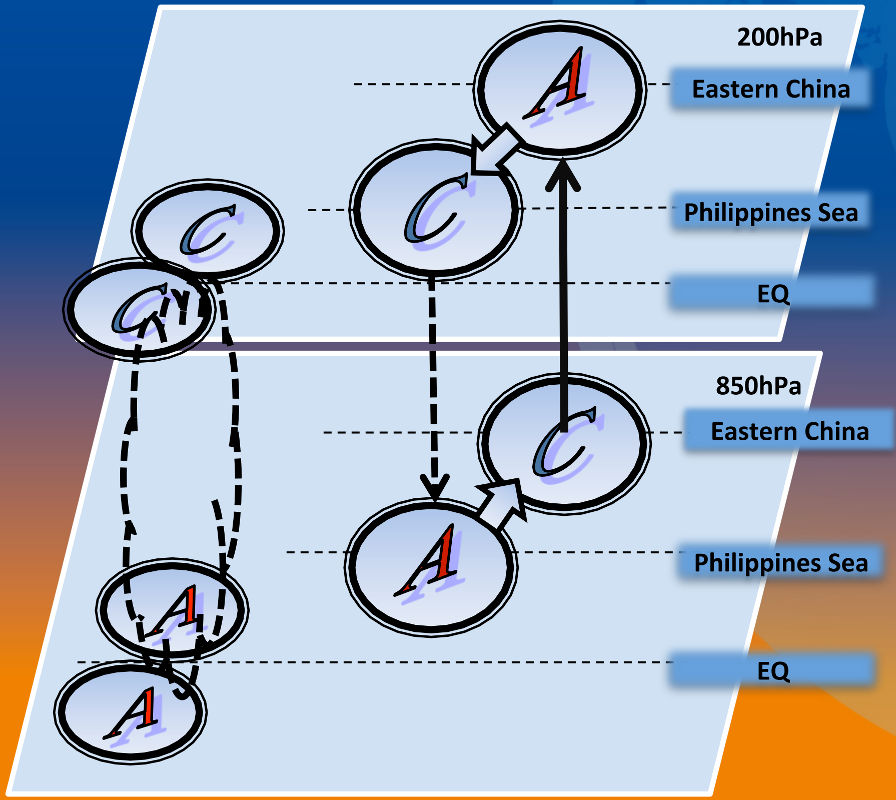

Anomalous ω (contour) and integrated precipitable water

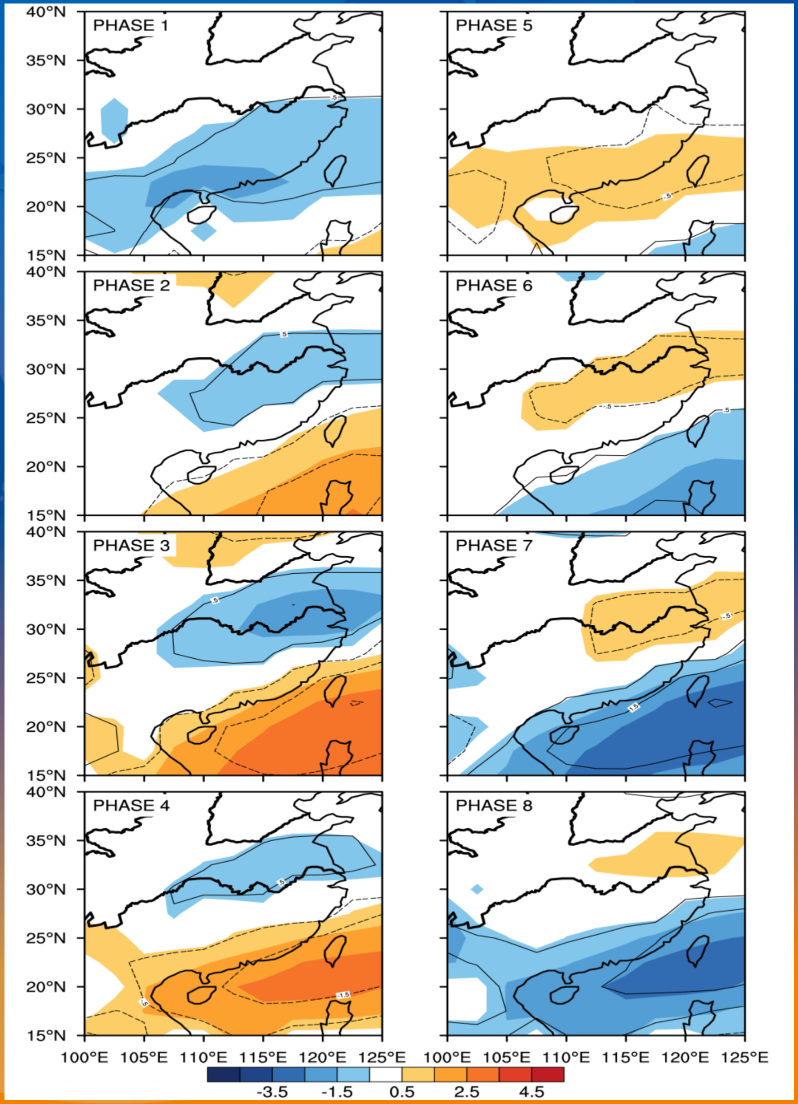

Case study of the impact on the Yantze rainfall of both 30-60-day and 10-30-day BSISOs during the 1996 summer

Li, Mao, and Wu (2015, CD)

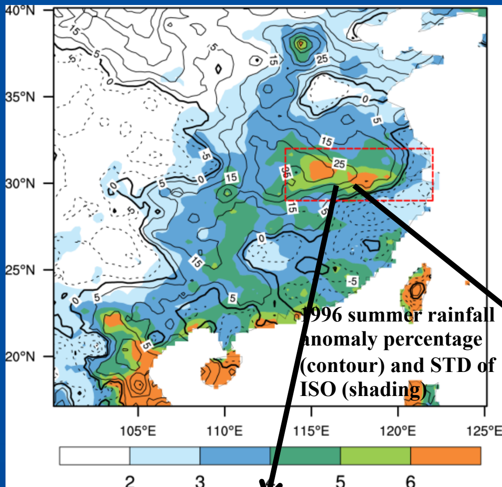

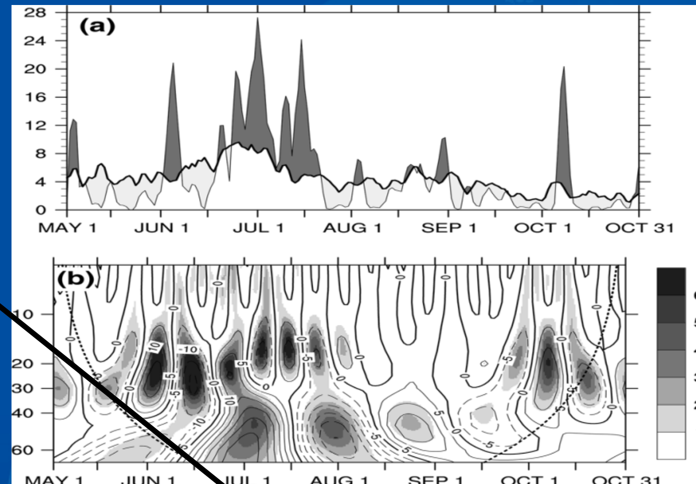

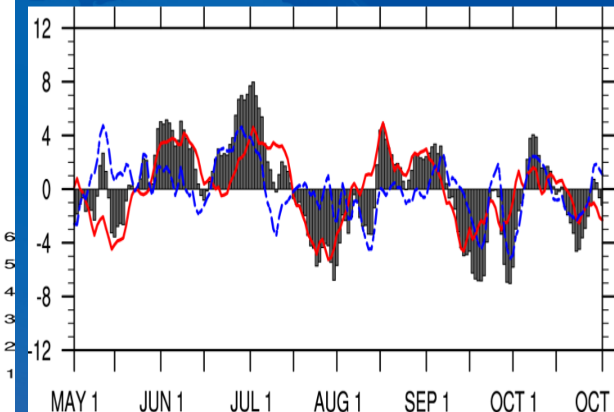

30-60-day BSISO1

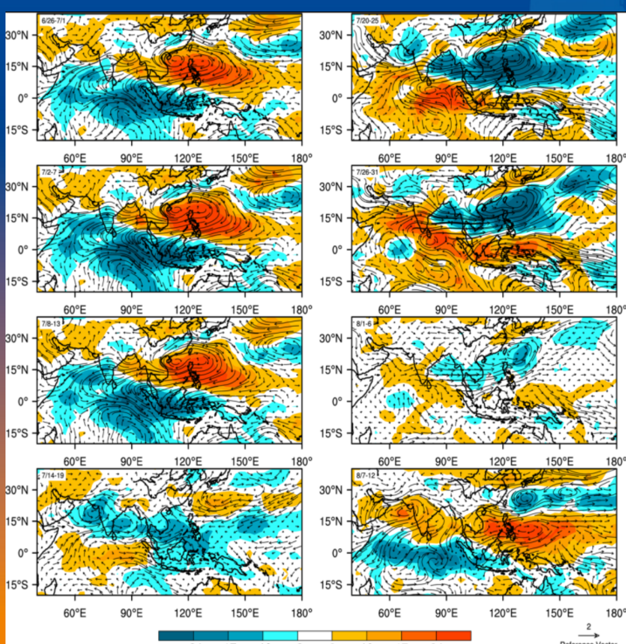

10-30-day BSISO2

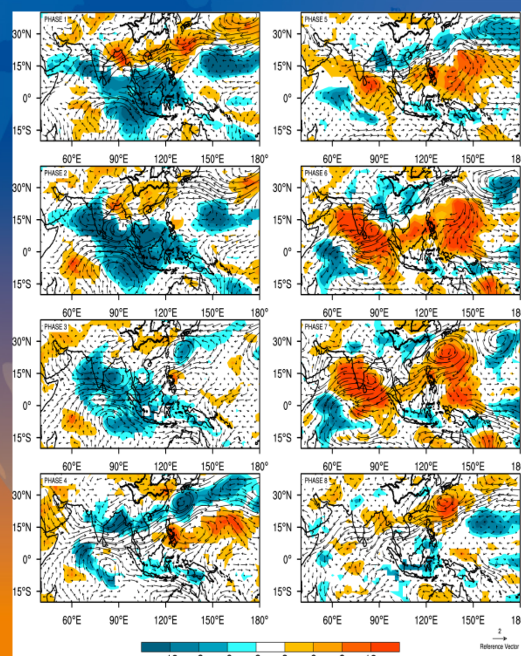

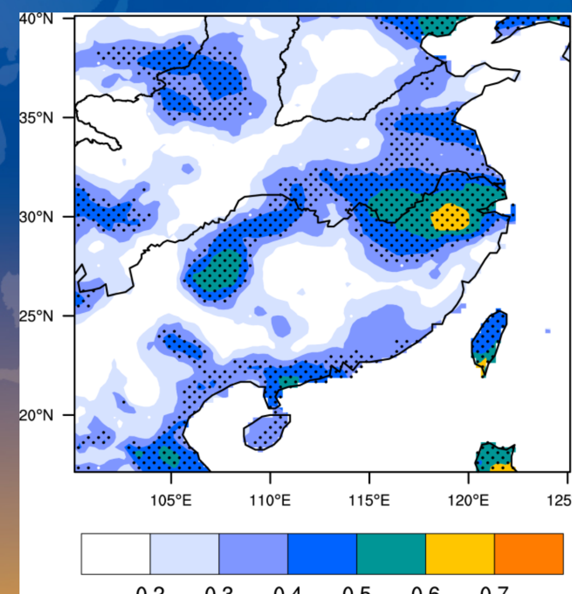

Correlation between Multivariate regressing forecasted and observed rainfall anomalies

Interaction of the 30-60-day BSISO with extratropical ISO around Tibetan Plateau and their coordinated influence the 1998 Yangtze flooding

Li and Mao (2017)

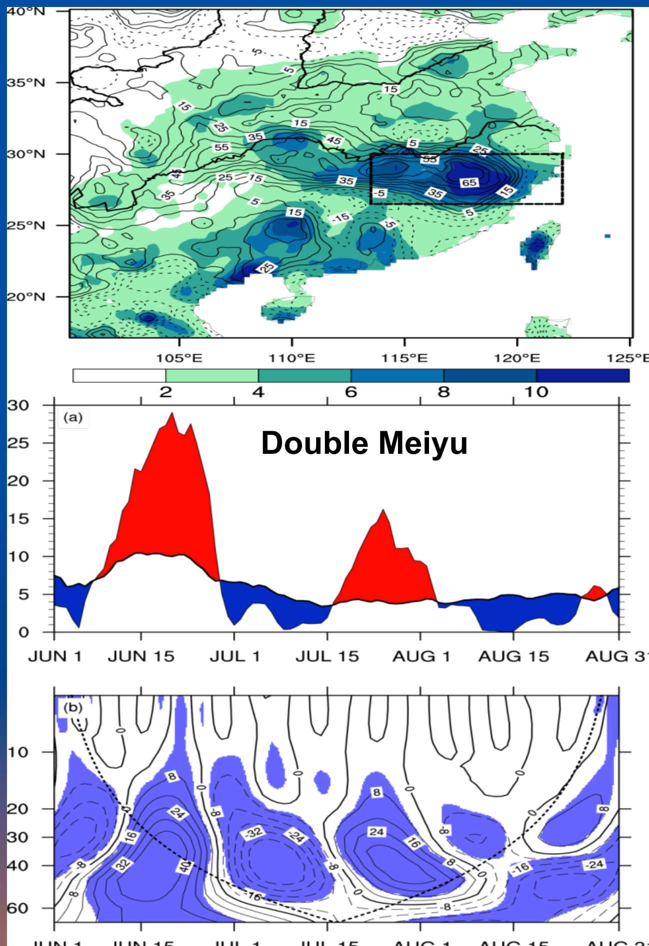

200hPa 30-60-day filtered vorticity (contour) and divergent winds (vectors) and OLR (shading) anomalies

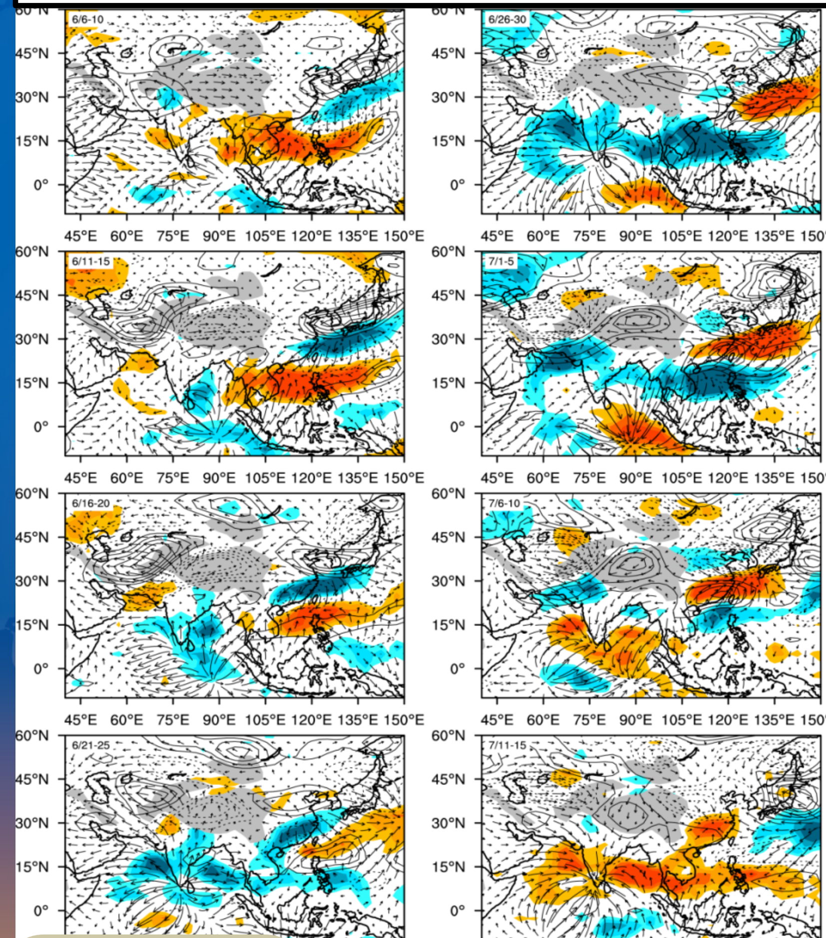

$$\frac{\partial \varsigma}{\partial t} = -\vec{V}_{\psi} \cdot \nabla \xi - (\xi \nabla \cdot \vec{V}_{\varphi} + \vec{V}_{\varphi} \cdot \nabla \xi) + \frac{(f+\xi)}{\theta_z}\frac{\partial Q}{\partial z} - \left(\frac{1}{\theta_z}\frac{\partial v}{\partial z}\frac{\partial Q}{\partial x} - \frac{1}{\theta_z}\frac{\partial u}{\partial z}\frac{\partial Q}{\partial y}\right)$$

Advection

Rossby wave source related to upper-tropospheric BSISO divegent winds

Voticity creation due to vertical non-uniform diabatic heating

Voticity creation due to horizontal non-uniform diabatic heating

Wu and Liu (1997)

$$\frac{\partial \varsigma}{\partial t} \propto -\vec{V}_{\psi} \cdot \nabla \xi$$

$$\frac{\partial \varsigma}{\partial t} \propto -(\xi * \nabla \cdot \vec{V} + \vec{V}_{\varphi} \cdot \nabla \xi)$$

Rossby wave source

$$\frac{\partial \varsigma}{\partial t} \propto \frac{(f+\xi)}{\theta_z} \frac{\partial Q}{\partial z}$$

$$\frac{\partial \varsigma}{\partial t} \propto -\left(\frac{1}{\theta_z} \frac{\partial v}{\partial z} \frac{\partial Q}{\partial x} - \frac{1}{\theta_z} \frac{\partial u}{\partial z} \frac{\partial Q}{\partial y}\right)$$

Yangtze Wet phase | **Dry phase**

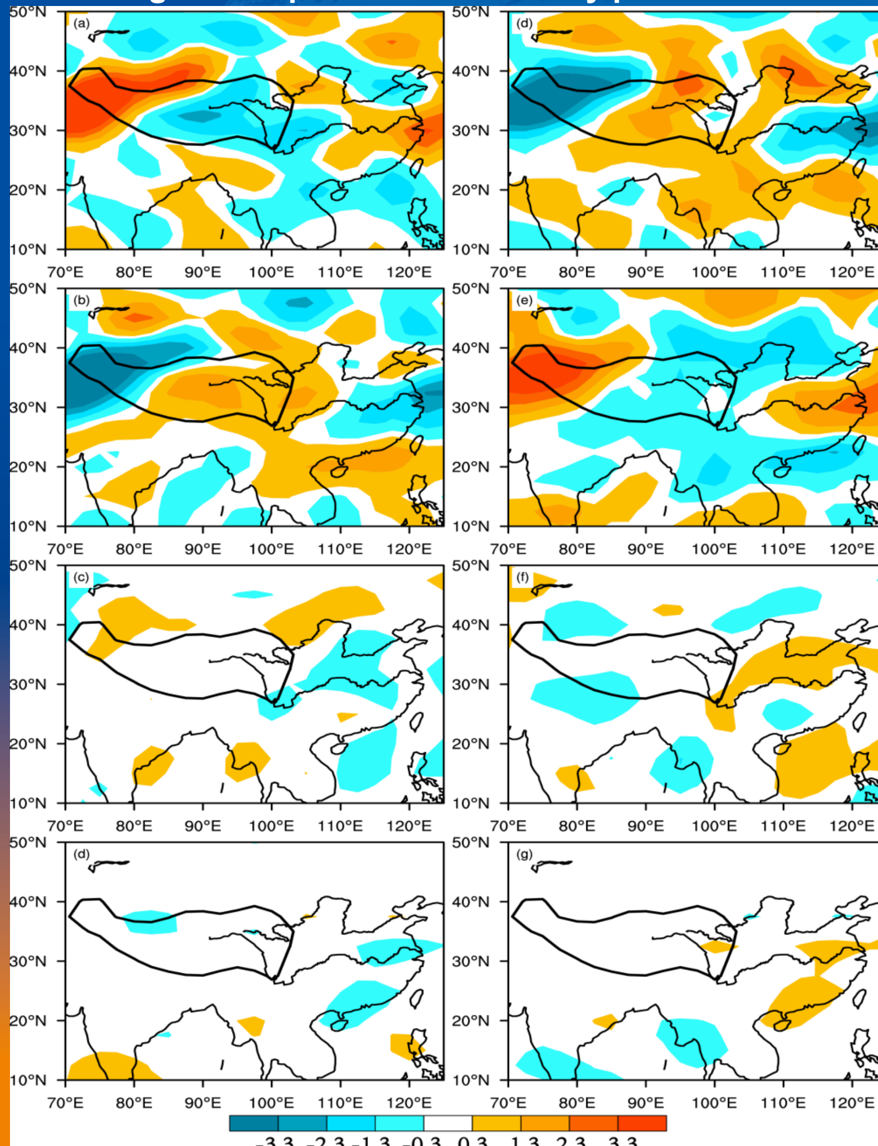

→ Favor westward propagation of ISO

→ Increasing positive vorticity over TP, negative Vorticity over Yangtze, keep divergent condition

Year-to-year difference in BSISO impact over eastern China

Li and Mao (2016)

Percentage rianfall anomaly (contour）
Standard Deviation of intraseasonal rainfall （shading）

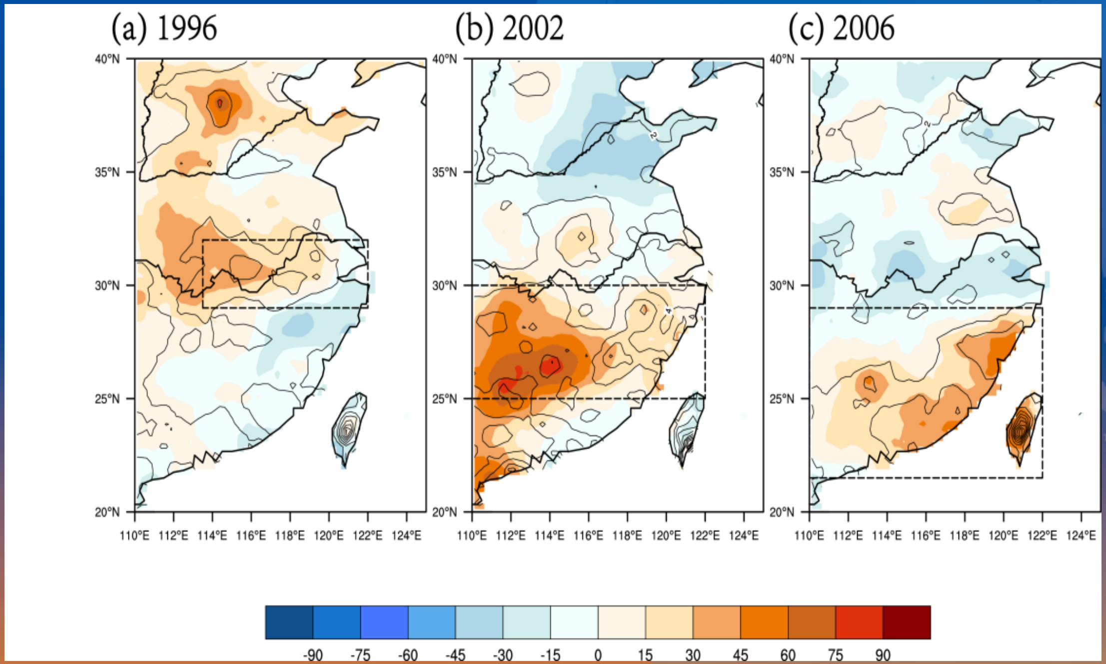

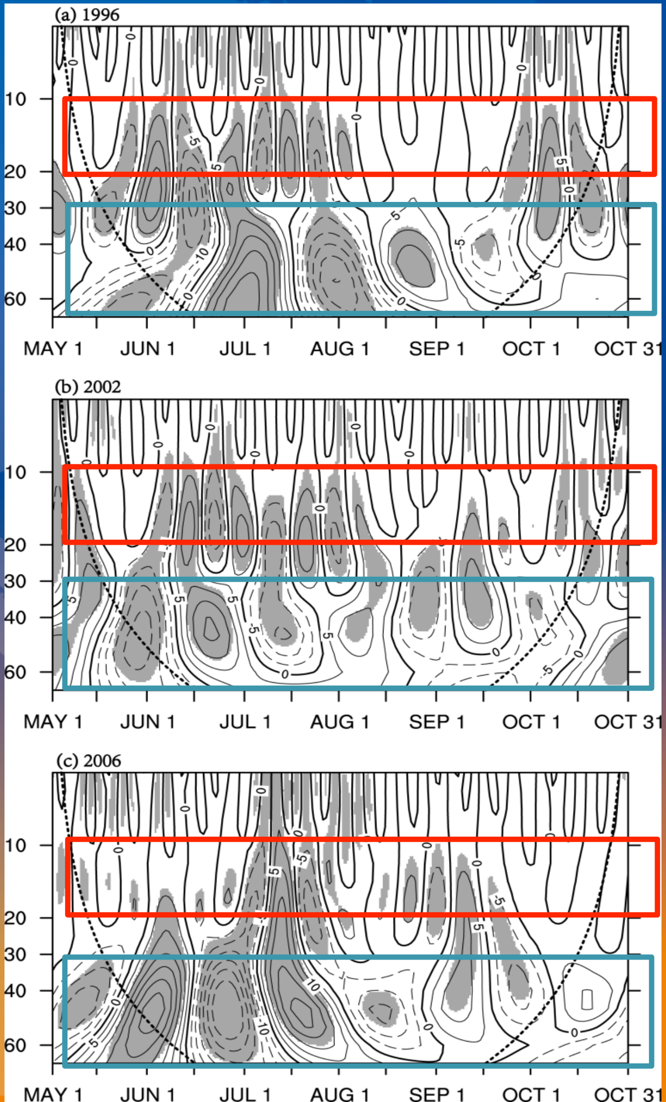

Three kind of distributions of larger intraseasonal rainfall variability appearing over different areas

Influence of IOD on the interannual variability of northward propagation of BSISO over South Asian Sector

Ajayamohan et al. (2008)

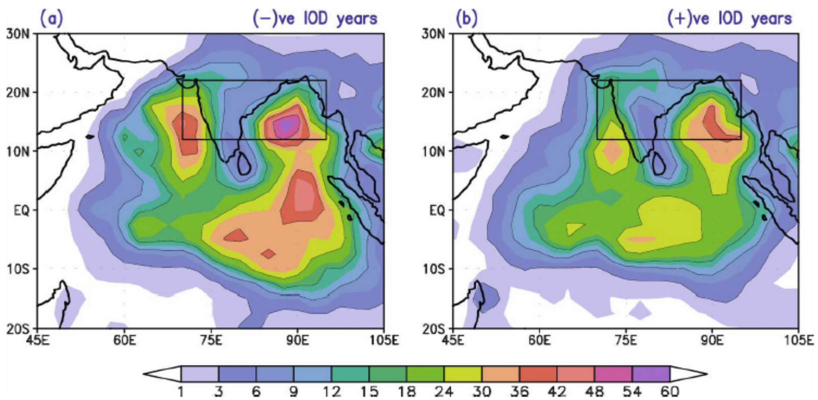

FIG. 2. (a) JJAS composite mean variance of 20–100-day filtered CMAP precipitation anomalies ($mm^2\ day^{-2}$) in contrasting IOD years (see Table 1 for the list of negative and positive IOD years). Contour levels are 3, 9, 15, 24, 36, 48, and 60. The box represents the base region (12°–22°N, 70°–95°E) taken for the regression calculations.

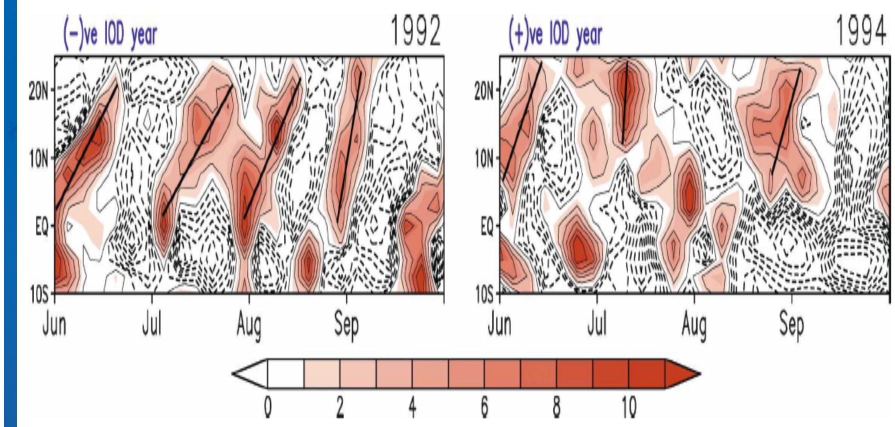

FIG. 3. Time–latitude plot of unfiltered (only annual cycle removed) precipitation anomalies ($mm\ day^{-1}$) averaged between 70° and 95°E during two typically contrasting IOD years. Slanted lines represent poleward-propagating anomalies that are well connected.

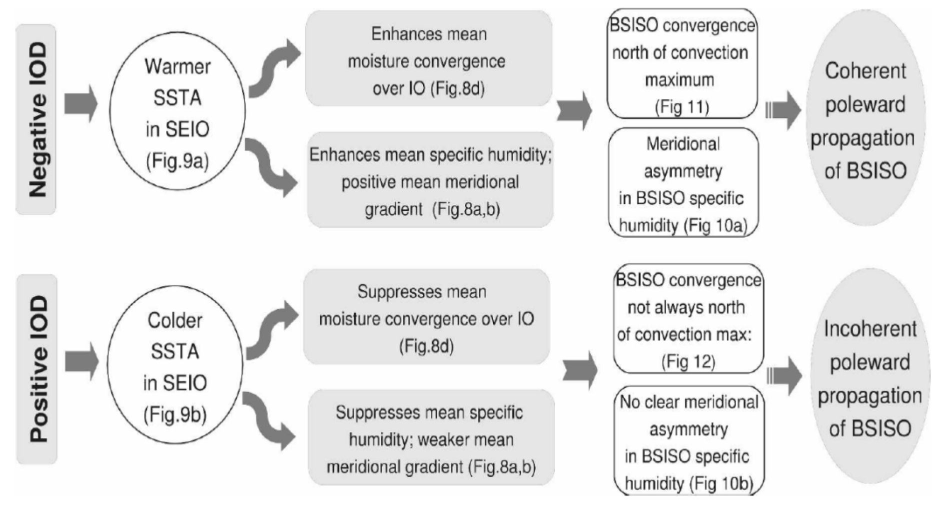

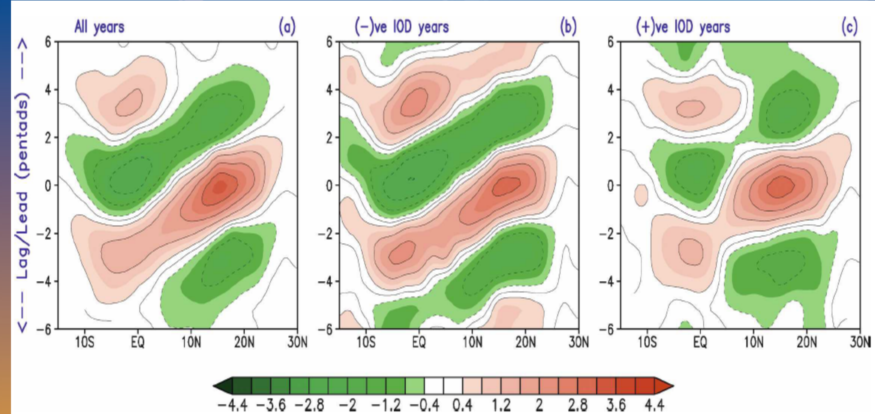

FIG. 6. (a) Regressed filtered anomalies of CMAP precipitation ($mm\ day^{-1}$) averaged over 70°–95°E as a function of latitude and time lag during the 1980–2004 period. As in (a), but for (b) negative and (c) positive IOD years. Contour interval is 0.6. Only statistically significant (0.1 significance level using a t test) anomalies are plotted.

Outline

1. Overview

2. Influences of BSISOs on rainfall anomalies over eastern China

3. Future changes of 30–60-day BSISO projected by CNRM-CM5 model

4. Summary

(IPCC; 2013)

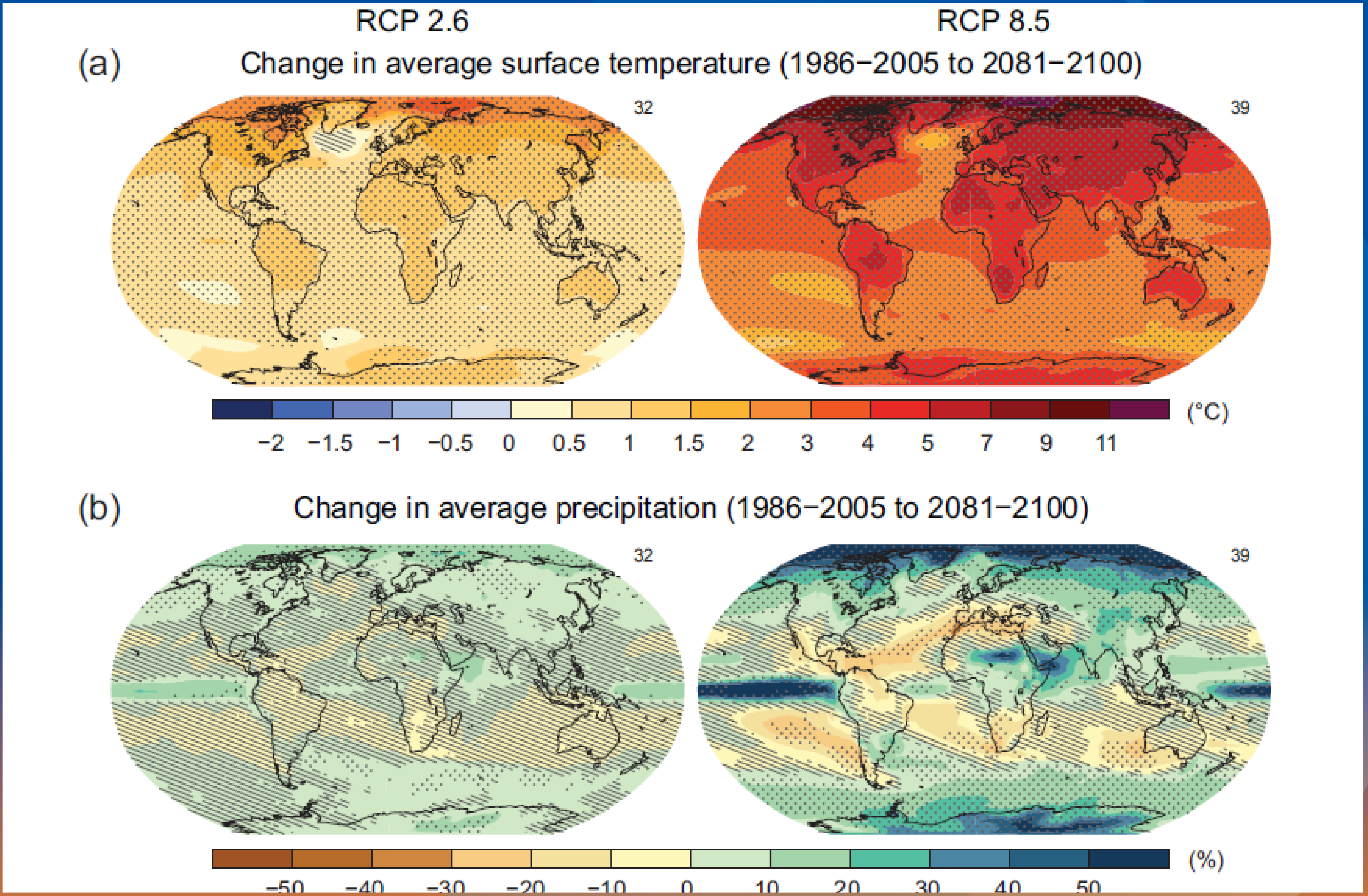

Global warming in the twenty-first century even under the RCP 2.6 scenario.

Simulation and Projection of MJO/BSISO

Some CGCMs are able to reproduce reasonably the structure and propagation of MJO/BSISO (especially **30-60-day BSISO**) based on evaluating the simulation performance of CMIP3 (Meehl et al. 2007) and **CMIP5** (Taylor et al. 2012) CGCMs.

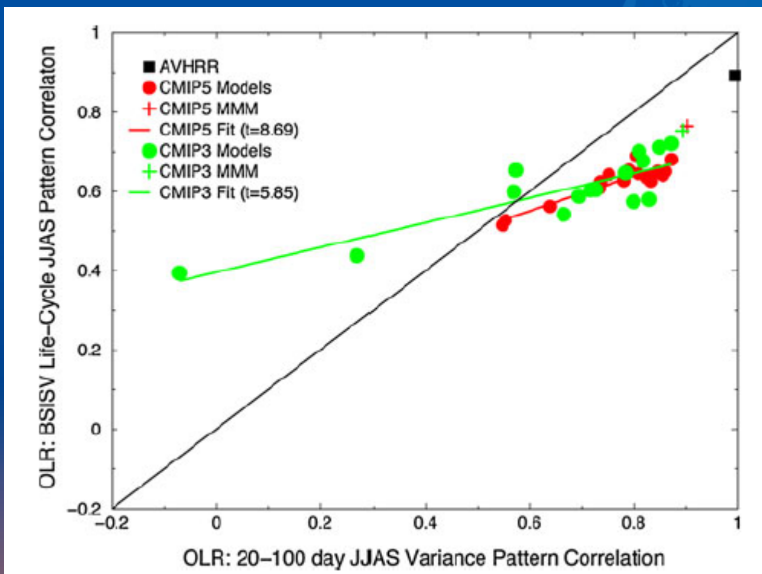

Sperber et al. 2013

Table 2. The Capability of the 32 Models to Simulate the Important Aspects of the BSISO Is Either Denoted With Yes or No[a]

Model	Realistic Spatial Pattern of Climatological JJAS Mean Precipitation (Figure 4)	Realistic Spatial Pattern of BSISO Variance (Figure 7)	Eastward Propagating Mode Over the Equatorial Indian Ocean (Figure 8)	Realistic Northward Propagation of the BSISO (Figure 9)	Realistic Space Time Structure of Northward Propagating Mode (Figure 10)	Tilted Rain Band (Figure 12)	Evolution of BSISO Life Cycle (Movie)
ACCESS1.0	No	No	Yes	Yes	No	No	correct
ACCESS1.3	No	No	Yes	No	No	No	correct
BCC-CSM1.1	No	No	Yes	No	No	No	correct
CanCM4	Yes	No	Yes	Yes	No	No	correct
CanESM2	Yes	No	Yes	Yes	No	No	correct
CCSM4	No	No	Yes	No	No	No	wrong
CESM1(BGC)	No	No	No	No	No	No	wrong
CESM1(FAST CHEM)	No	No	Yes	No	Yes	No	wrong
CMCC-CM	***No***	***No+***	***Yes***	***Yes***	***Yes***	***Yes***	***correct***
CNRM-CM5	Yes	No	Yes	Yes	Yes	Yes	wrong
CSIRO-Mk3.6.0	No	Yes	Yes	No	Yes	No	correct
GFDL-CM3	***Yes***	***No***	***Yes***	***Yes***	***Yes***	***Yes***	***correct***
GFDL-ESM2G	Yes	No	Yes	Yes	No	Yes	correct
GFDL-ESM2M	Yes	No	Yes	Yes	No	Yes	correct
HadCM3	No	No	Yes	Yes	No	No	correct
HadGEM2-CC	No	No	Yes	No	No	No	correct
HadGEM2-ES	No	No	Yes	No	No	No	correct
INM-CM4	No	No	Yes	No	No	No	wrong
IPSL-CM5A-LR	***Yes***	***No***	***Yes***	***Yes***	***Yes***	***Yes***	***correct***
IPSL-CM5A-MR	Yes	No	Yes	No	No	No	correct
IPSL-CM5B-LR	No	No	Yes	No	No	No	wrong
MIROC4h	No	No	No	No	No	No	wrong
MIROC5	***No***	***No+***	***Yes***	***Yes***	***Yes***	***Yes***	***correct***
MIROC-ESM	No	No	Yes	No	Yes	No	correct
MIROC-ESM-CHEM	No	No	Yes	No	Yes	No	wrong
MPI-ESM-LR	***Yes***	***Yes+***	***Yes***	***Yes***	***Yes***	***Yes***	***correct***
MPI-ESM-MR	Yes	Yes+	Yes	Yes	No	Yes	wrong
MPI-ESM-P	Yes	Yes+	Yes	Yes	No	Yes	wrong
MRI-CGCM3	No	No	Yes	No	No	No	correct
NorESM1-M	No	No	Yes	No	No	No	wrong
BNU-ESM	Yes	No+	Yes	No	No	No	wrong
FGOALS-s2	No	No	Yes	No	No	No	wrong

Sabeerali et al. 2013

□**Scientific Issue: How will the 30-60-day BSISO change under extreme scenario of RCP8.5?**

Capability of 24 CMIP5 models to simulate the important aspects of the BSISO

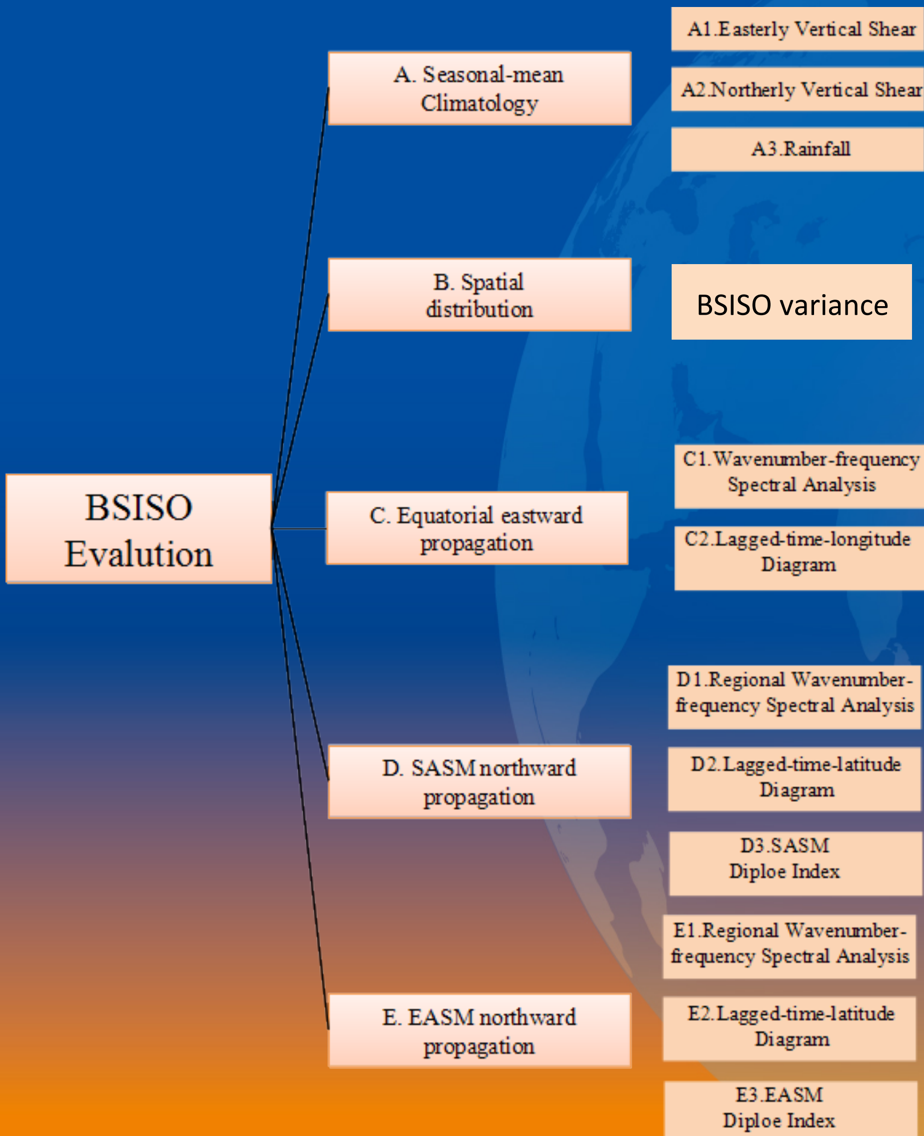

Evalution Scheme

$$Wgt = \frac{Wgt_{A1} + Wgt_{A2} + Wgt_{A3}}{3} + Wgt_{B1} + \frac{Wgt_{C1} + Wgt_{C2}}{2} + \frac{Wgt_{D1} + Wgt_{D2} + Wgt_{D3}}{3} + \frac{Wgt_{E1} + Wgt_{E2} + Wgt_{E3}}{3}$$

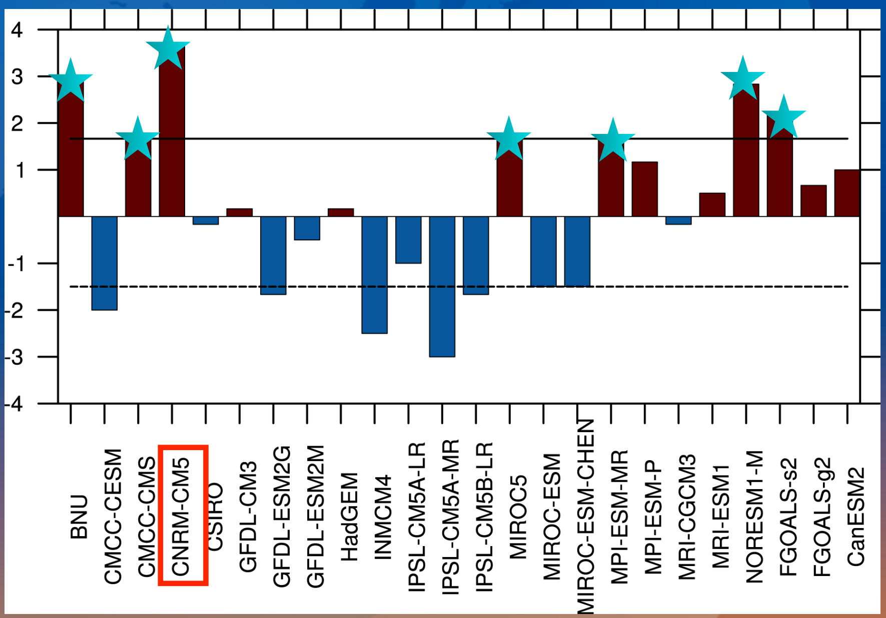

Historical Run (20 century)

VS

RCP 8.5 (21 century)

CNRM-CM5 (T127L31; 1.4°×1.4°; Voldoire et al. 2013) by CNRM-Cerfacs, France

3. 1 Future changes in boreal summer-mean state

SST (shading) & Specific Humidity

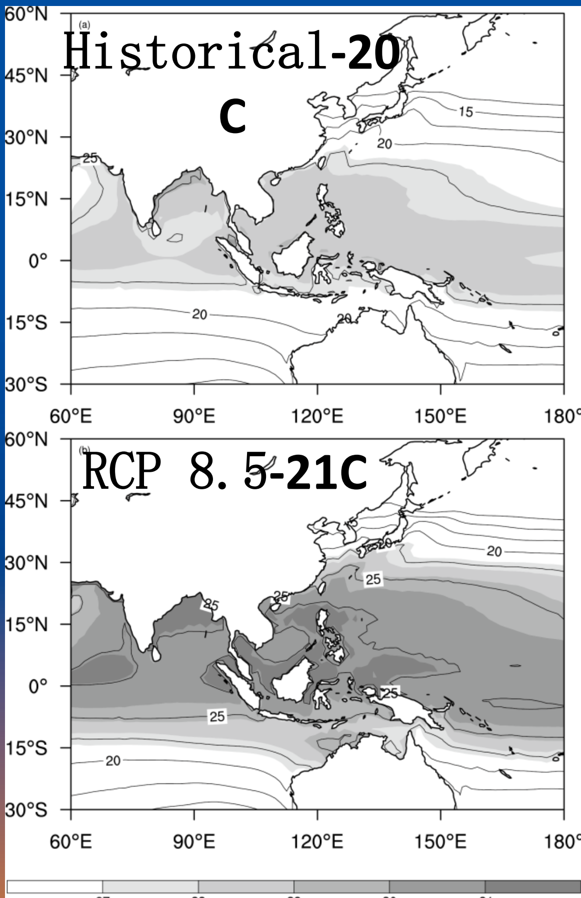

Rainfall and 850hPa winds

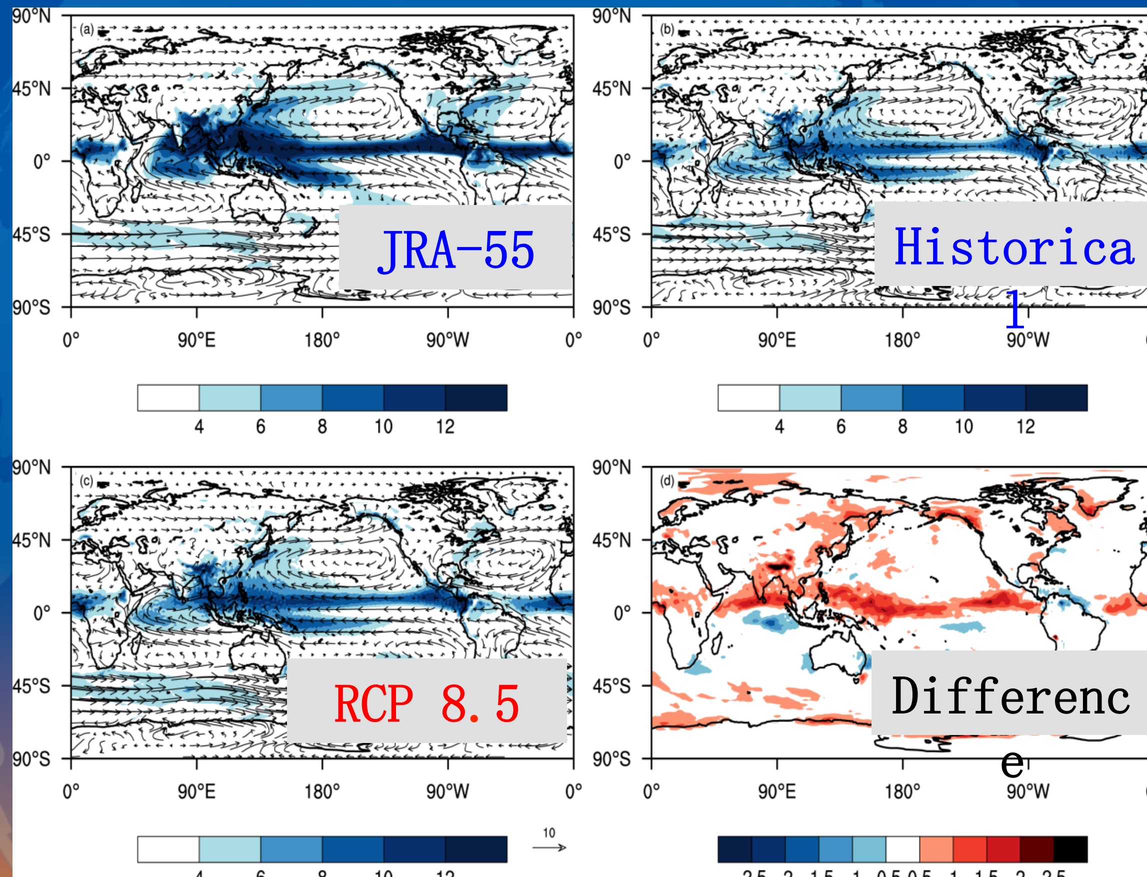

Li and Mao (2015)

Tropical convection centers generally occur over the areas of higher SST. High SST increase water vapor in the low-atmosphere, thereby increase the moist static energy, thus favoring convections to arise.

3. 1 Future changes in boreal summer-mean state

Clausius–Clapeyron equation for the atmospheric water vapor

$$\frac{des}{dT} = \frac{L_v e_s}{R_v T^2}$$

Saturation Vapor Pressure (e_s)

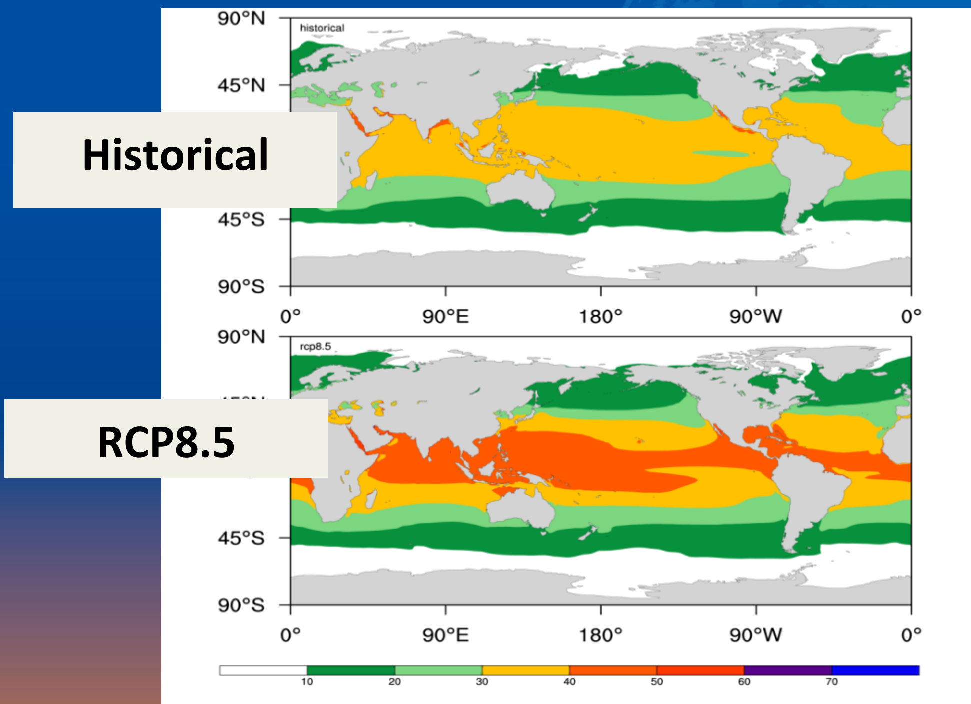

Saturation Specific Humidity (q_s)

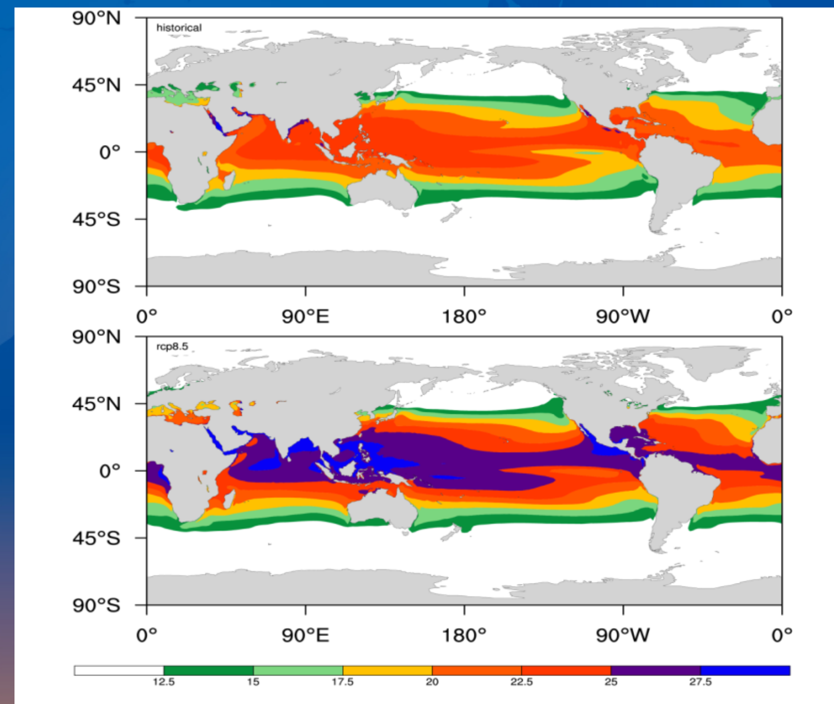

Increased SST → enhanced saturation water vapor pressure → more moisture into the low-level atmosphere, → favoring stronger tropical convection

As the saturation vapor pressure increases by about 7% for each 1-K warming in SSTs (Held and Soden, 2006), a 16% increase will arise in e_s, with q_s increasing to above 27.5 g/kg.

3.2 Future changes in the BSISO

◆ **BSISO amplitude**

Li and Mao (2015)

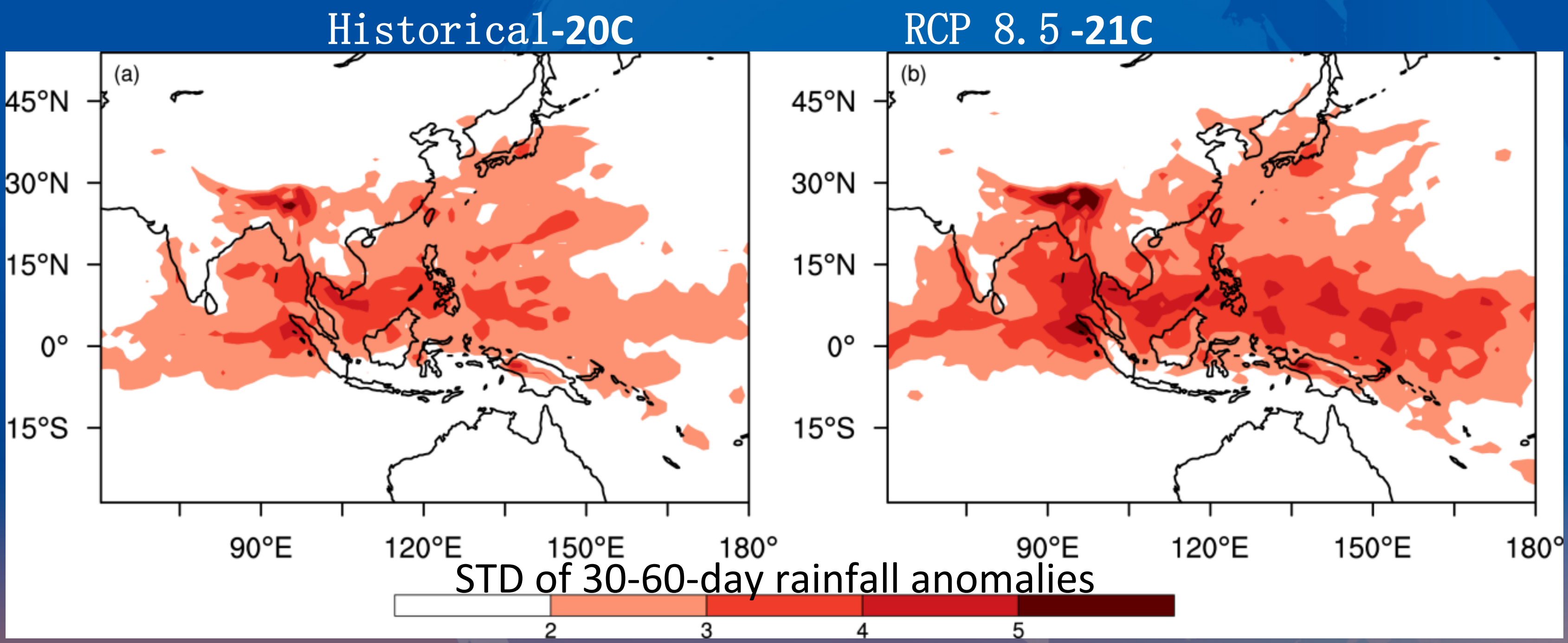

Enhanced Variability between equator and 15N

Expanded range (more eastward extension)

The northward/northwestward propagation over EA/WNP

3.2 Changes in the BSISO

◆ Equatorial Eastward Propagation **component from Indian to Pacific Oceans**

Zonal **Wavenumber-frequency power spectra over the** equatorial **region (10°S–25°N)**

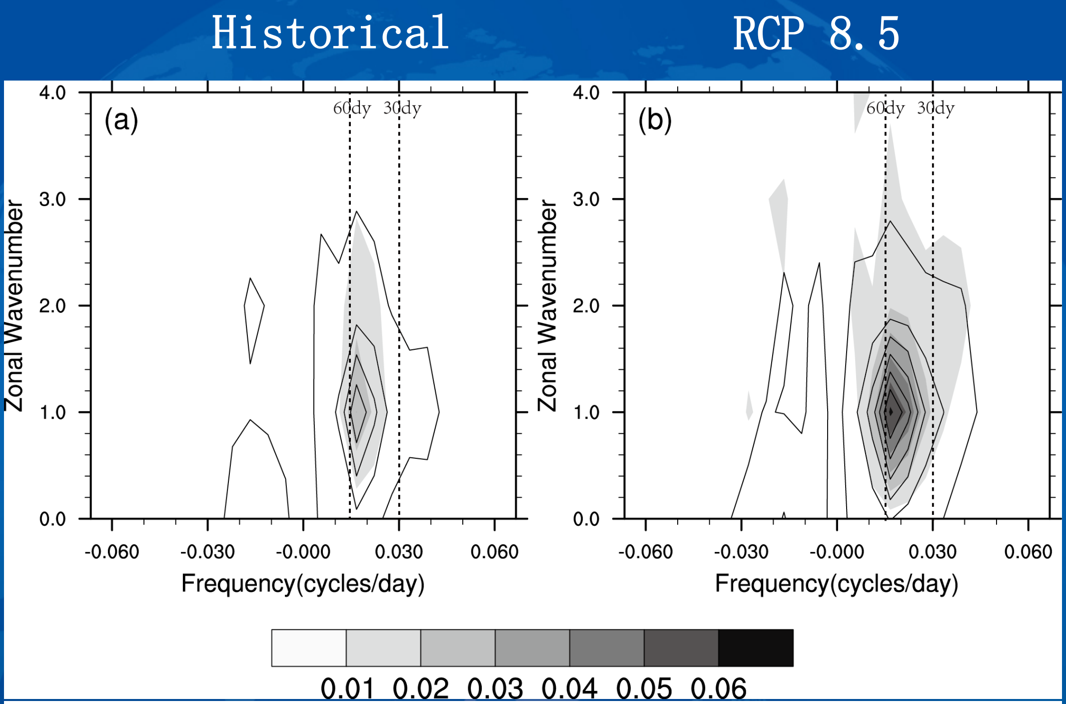

lagged-time-longitude diagram

Base point: **EIO (10°S–5°N,75–100°E)**

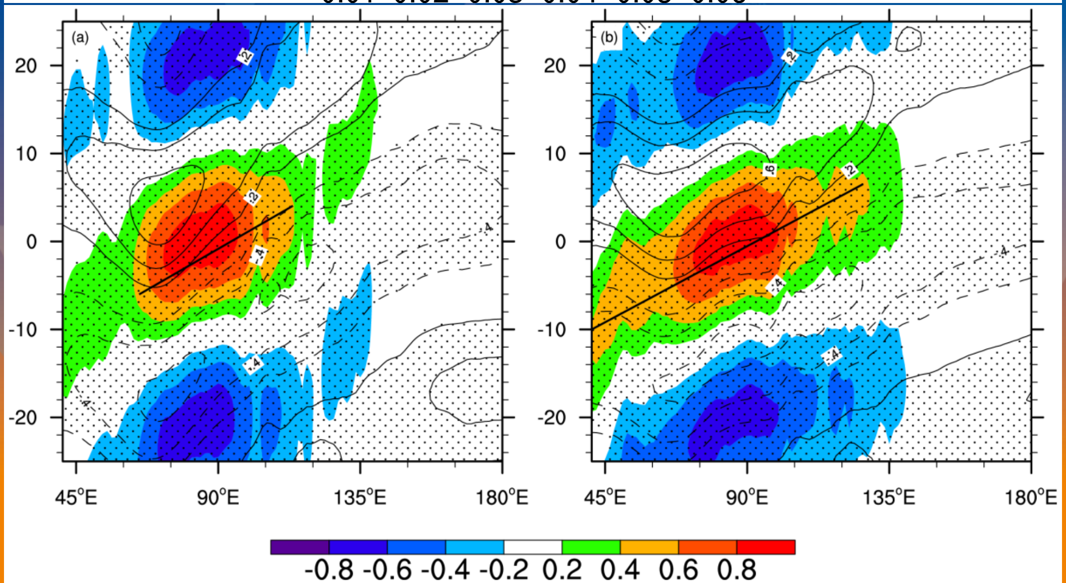

3.2 Changes in the BSISO over South Asia Sector

Historical (20C) RCP 8.5 (21C)

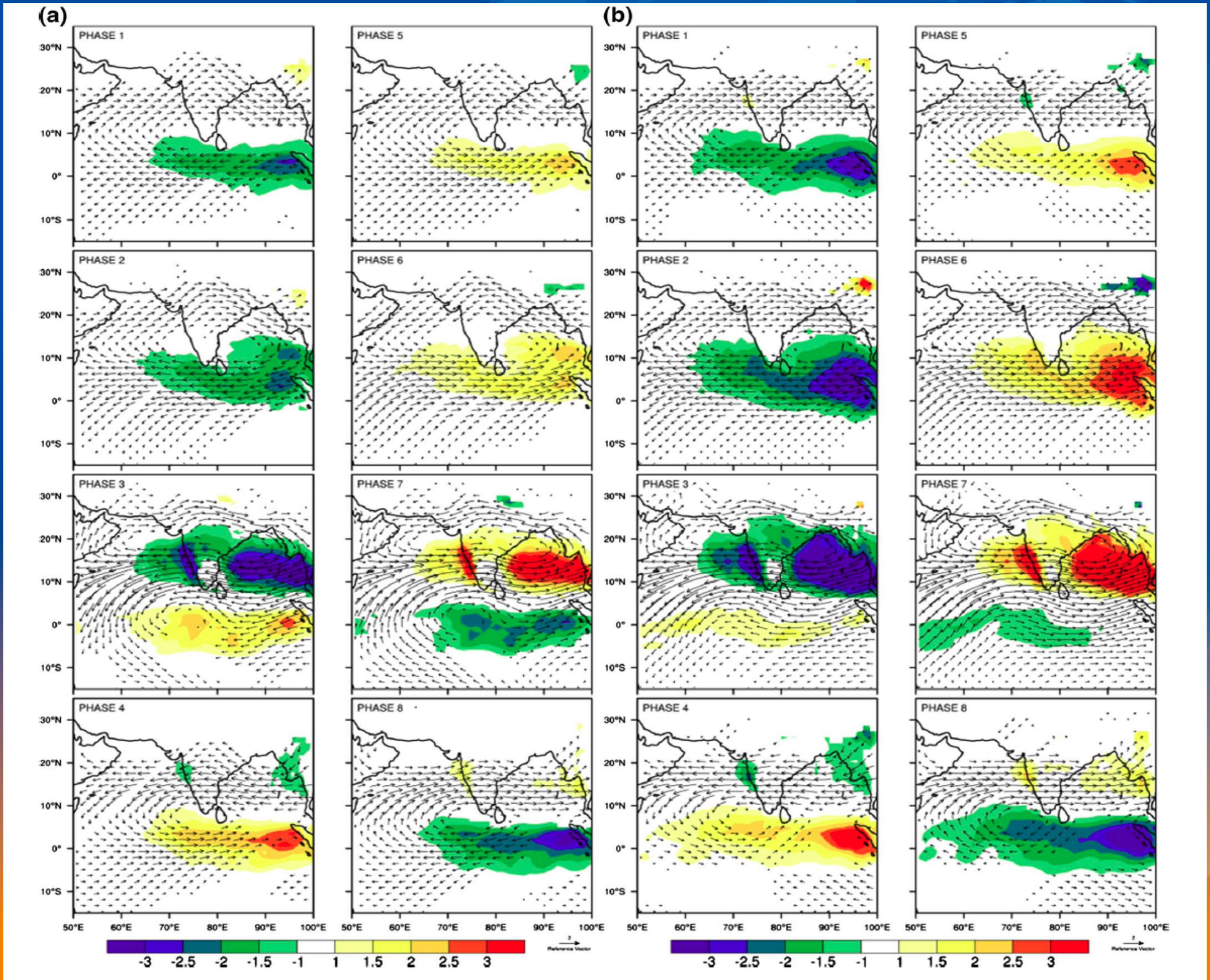

3.2 Changes in the BSISO over South Asia Sector

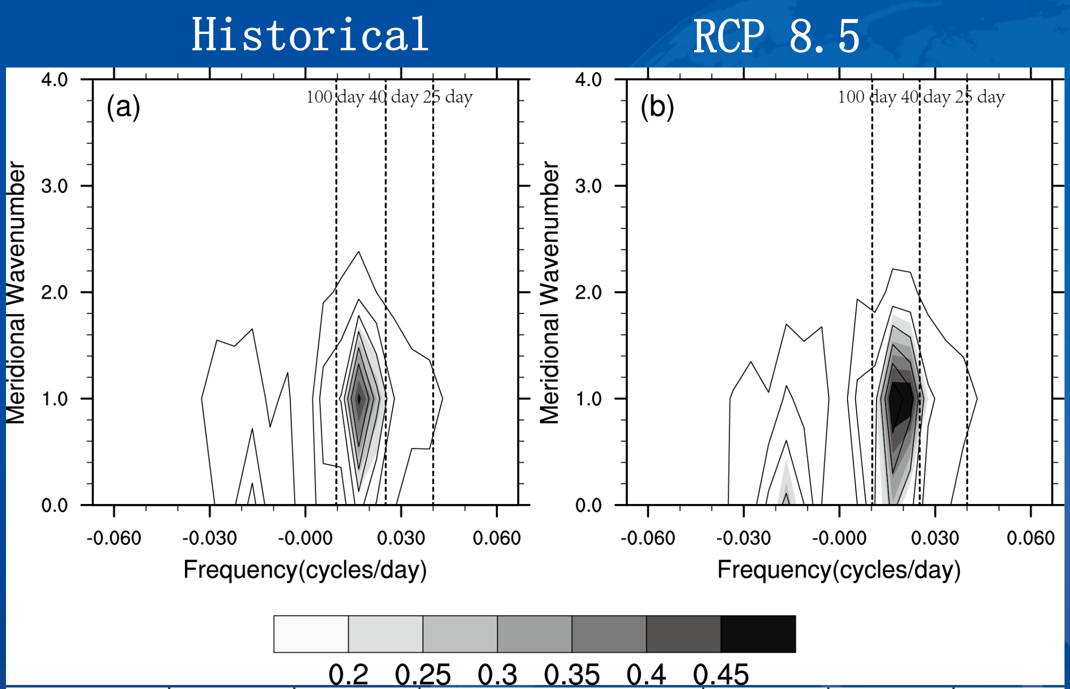

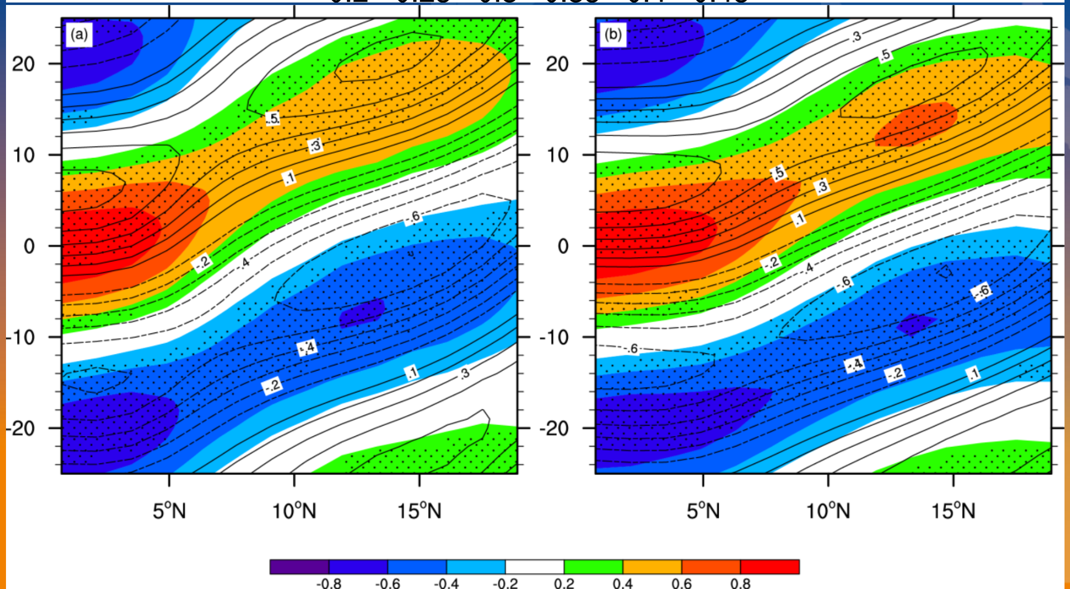

◆ **Northward Propagating Component over South Asian Sector**

Finite Domain **Wavenumber-frequency power spectra over the** SASM **region (10°S–30°N, 70°–100°E)**

lagged-time-latitude diagram
Base point: **EIO (10°S–5°N,75–100°E)**

3.2 Changes in the BSISO over South Asia Sector

◆ Northward Propagation **Component in dynamical and thermal factors**

Li and Mao (2015)

Historical RCP 8.5

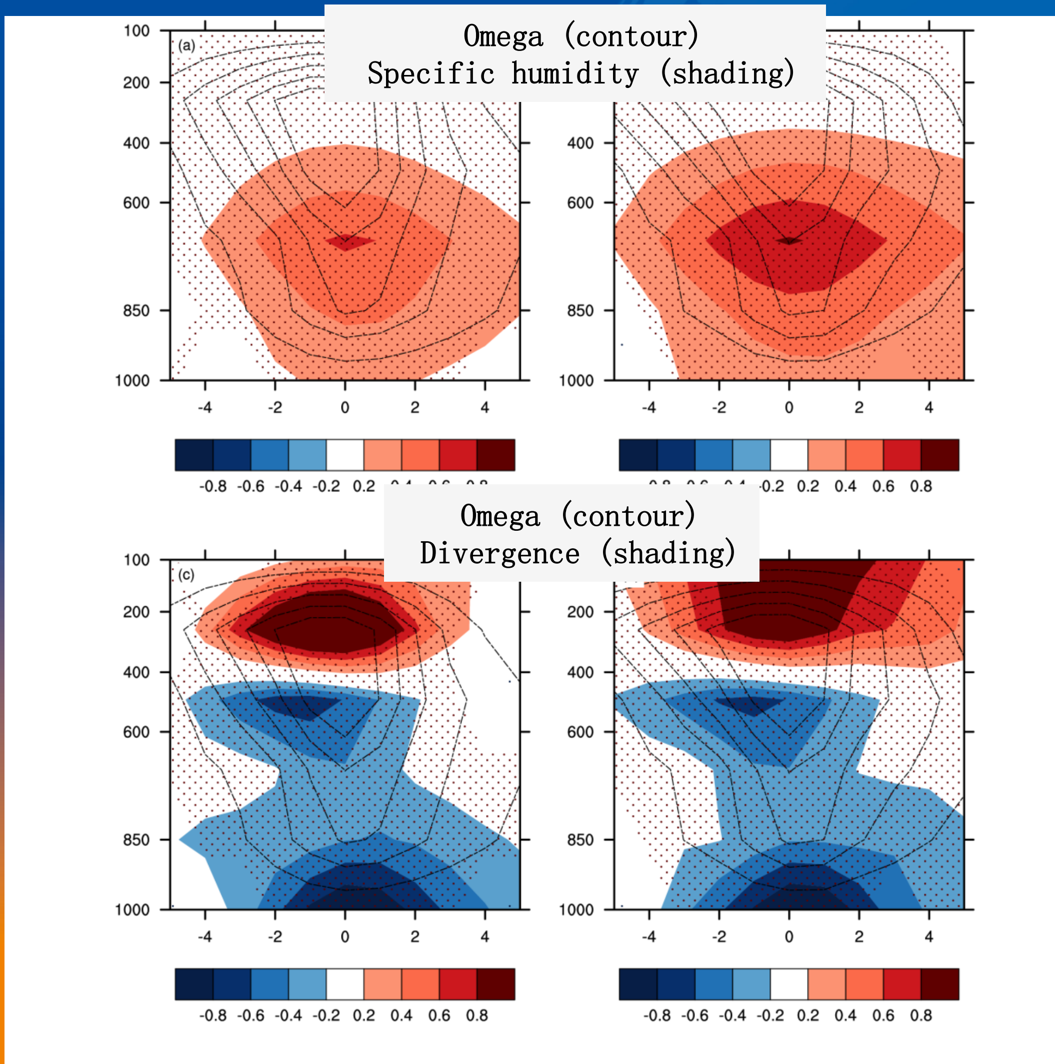

Influencing backgrounds:

Vertical easterly shear

Vorticity advection

Meridional ***asymmetry*** *of PBL specific humidity*

Convergence north of maximum convection

warmer and wetter PBL background

\+

stronger equatorial convection

→ stronger upward moisture transport

3.2 Changes in the BSISO over East Asia/WNP Sector

Historical (20C) RCP 8.5 (21C)

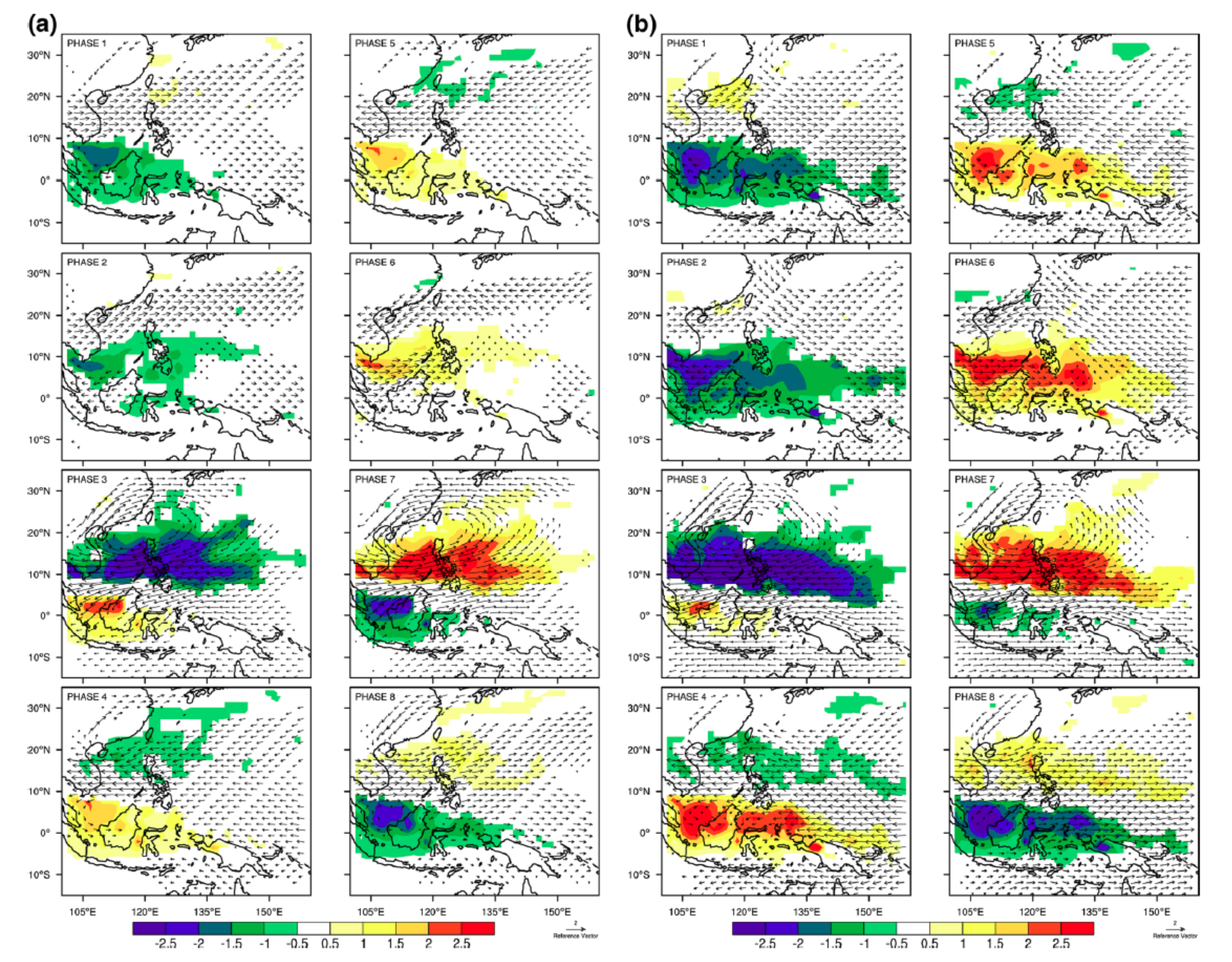

3.2 Changes in the BSISO over East Asia/WNP Sector

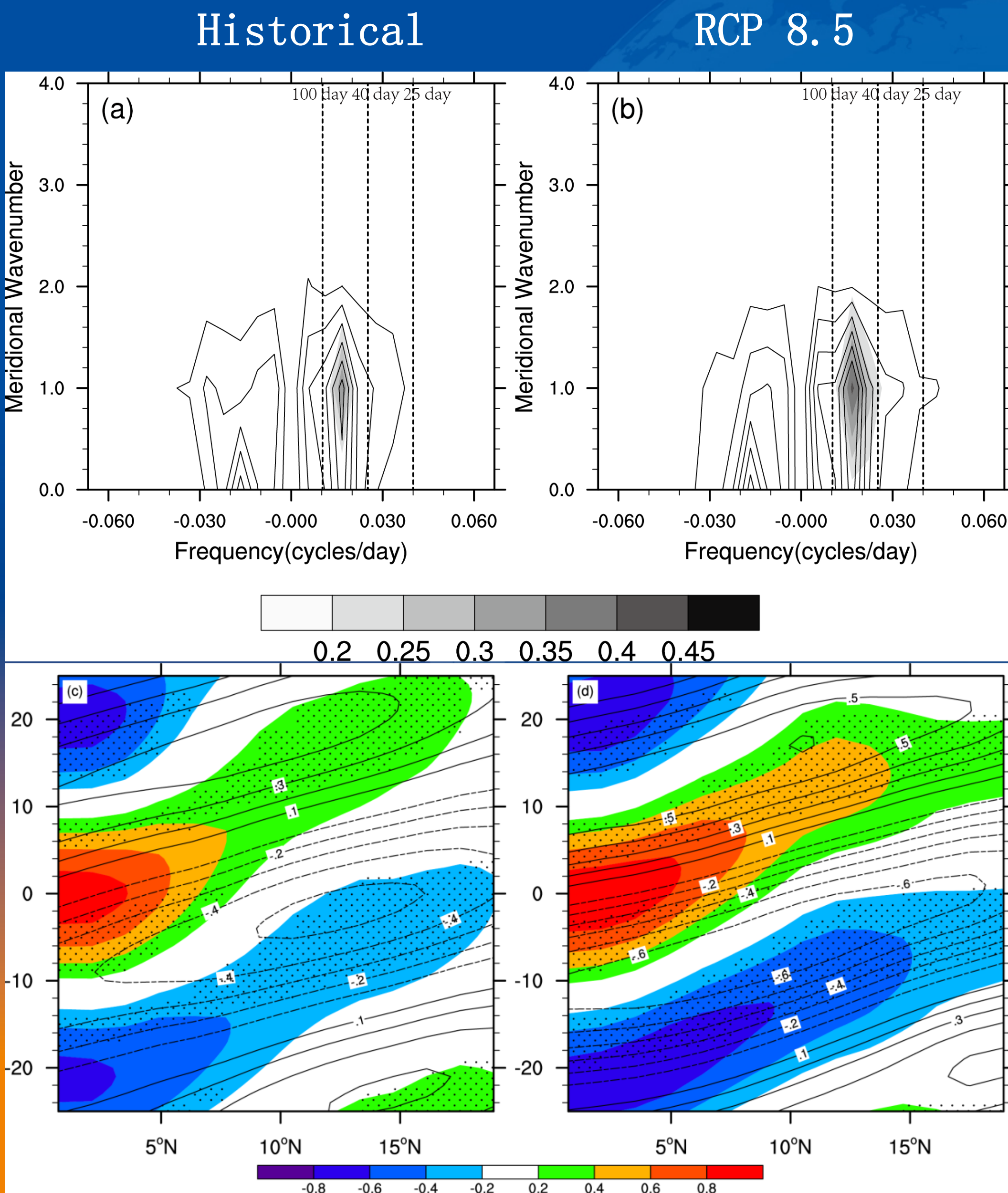

◆ **Northward Propagation Component over East Asian/WNP Sector**

Finite Domain **Wavenumber-frequency power spectra over the** EA/WNP **region (10°S–30°N, 100°–140°E)**

lagged-time-latitude diagram
Base point: **EWP (10°S–5°N,100–140°E)**

3.2 Changes in the BSISO over East Asia/WNP Sector

◆ Northward Propagation **Component in dynamical and thermal factors (Confirmed by Multi-model ensemble)**

Historical RCP 8.5

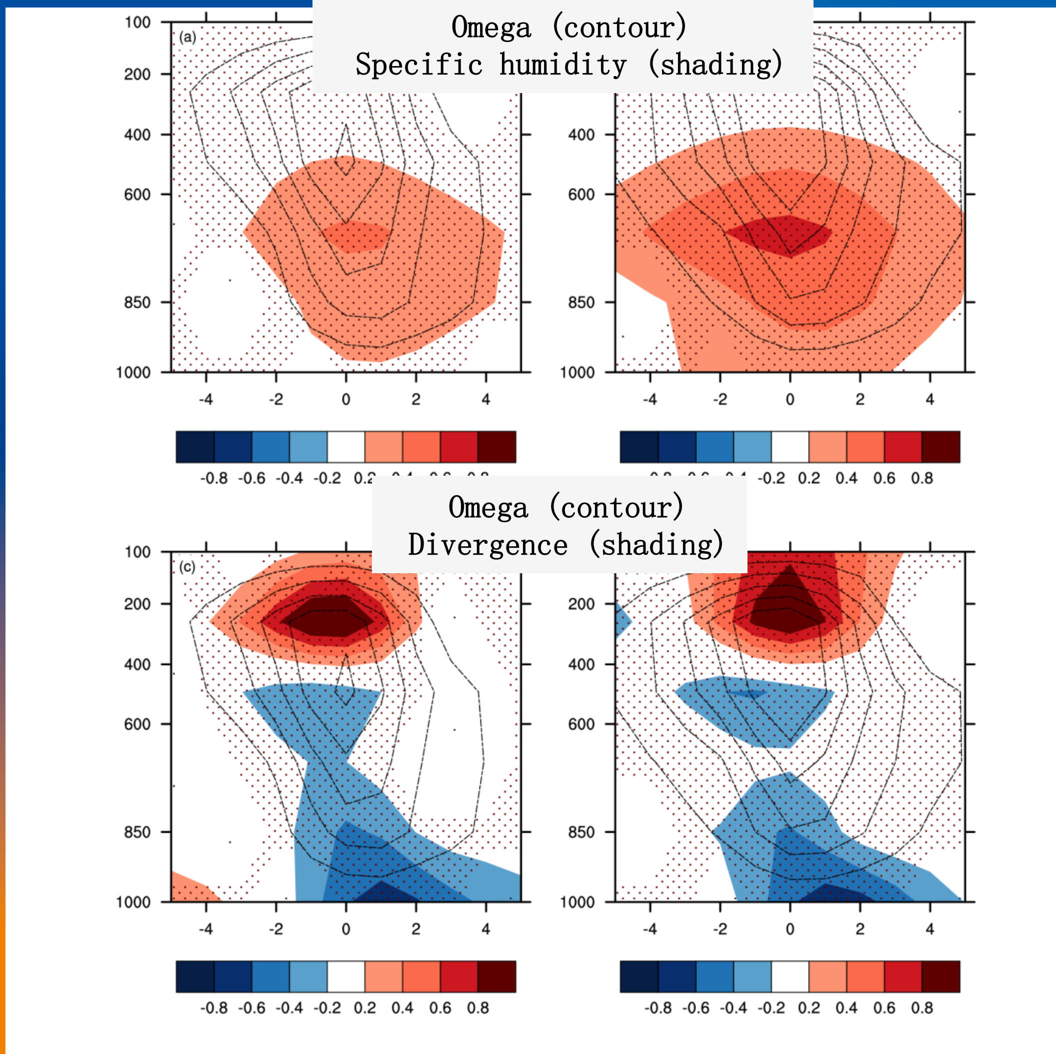

Influencing backgrounds:
vertical easterly shear
<u>vertical northerly shear</u>
meridional wind in the *PBL*
Meridional gradient of PBL specific humidity

warmer and wetter PBL background

\+

stronger equatorial convection

→ stronger upward moisture transport

Outline

1. **Overview**

2. **Influences of BSISOs on rainfall anomalies over eastern China**

3. **Future changes of 30–60-day BSISO projected by CNRM-CM5 model**

4. **Summary**

conclusions

1. **Intraseasonal rainfall anomalies over eastern China are closely phase-dependent on the evolutions of BSISOs, being caused by a local meridional–vertical cell.**
2. **Under RCP8.5 scenario,** the saturation **water vapor pressure** in the planetary boundary layer (PBL) **will** increase by about 16%**, as a** response to the increase of sea surface temperature **(SST)** in the tropical and subtropical Indian and Pacific Oceans, providing more moisture and moist static energy for tropical convection.
3. BSISO will be intensified, prevailing in a broader range of the Indo-Pacific region. The convective signal will initiate over more westward parts of the Indian Ocean and decay over the more eastward tropical Pacific.
4. Due to the increased moisture-holding capacity of the low-level atmosphere, the phase speeds of SASM and EA/WNP northward propagation will decrease.

Related Papers

- Jianying Li, Jiangyu Mao, Guoxiong Wu (2015) A Case Study of the Impact of Boreal Summer Intraseasonal Oscillations on Yangtze Rainfall. Clim Dym 44: 2683-2702 DOI: 10.1007/s00382-014-2425-9

- Jianying Li, Jiangyu Mao (2016) Experimental 15-day-Lead statistical forecast of intraseasonal summer monsoon rainfall over Eastern China. Atmospheric and Oceanic Science Letters 9: 66-73

- Jianying Li, Jiangyu Mao (2016) Changes in the boreal summer intraseasonal oscillation projected by the CNRM-CM5 model under the RCP 8.5 scenario. Clim Dym DOI: 10.1007/s00382-016-3038-2

Thank for your attention

LASG

Data and Method

Quadrupole Pattern

Li and Mao (2015)

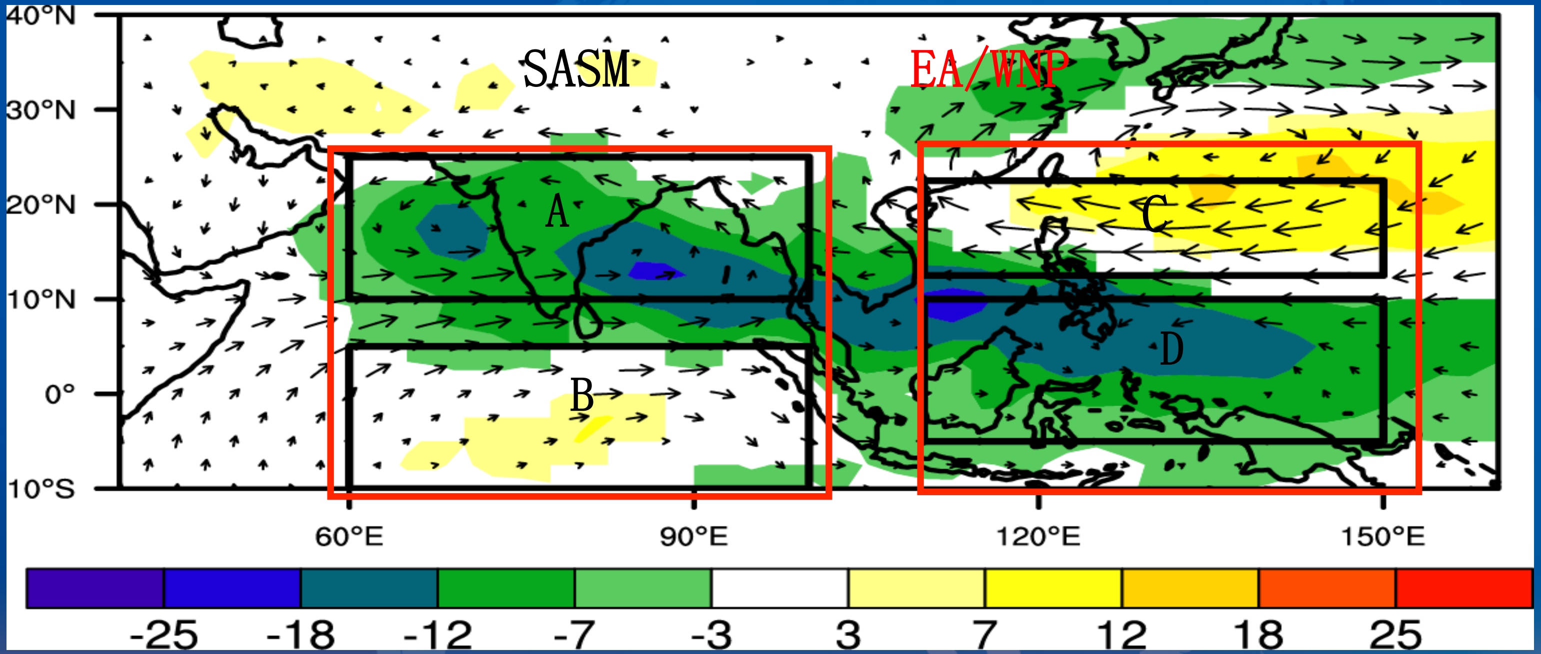

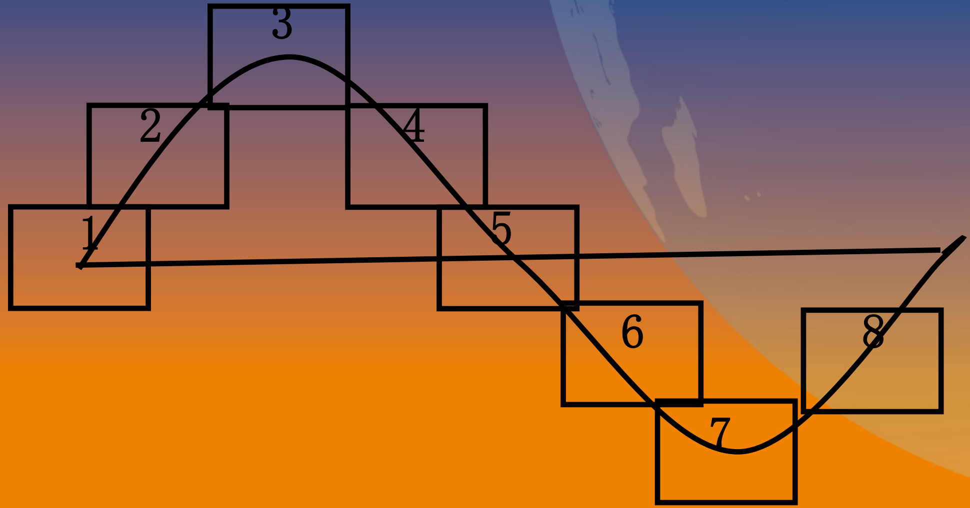

$$SADI(t) = A(t+nlag_{AB}) - B(t)$$

$$EADI(t) = C(t+nlag_{CD}) - D(t)$$

$$QPI(t) = SADI(t+nlag) - EADI(t)$$

亚洲夏季风30-60天季节内振荡的北传自组织机制

四极型指数定义

OLR & 850hPa 风场异常

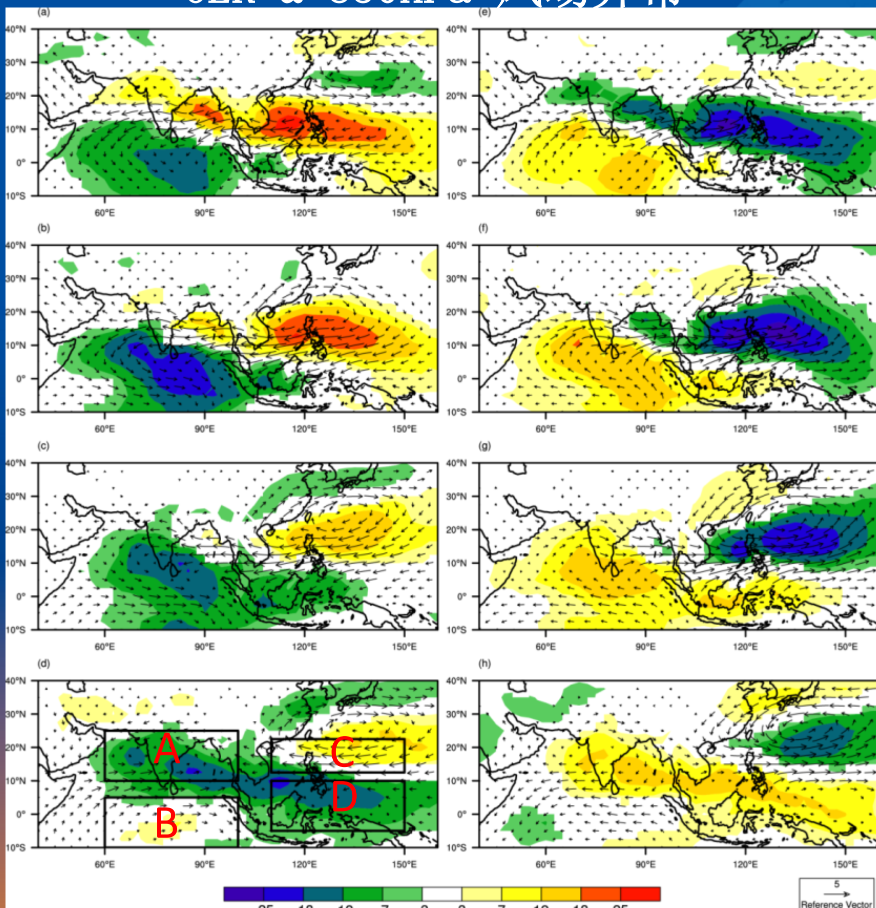

Lee et al. 2013

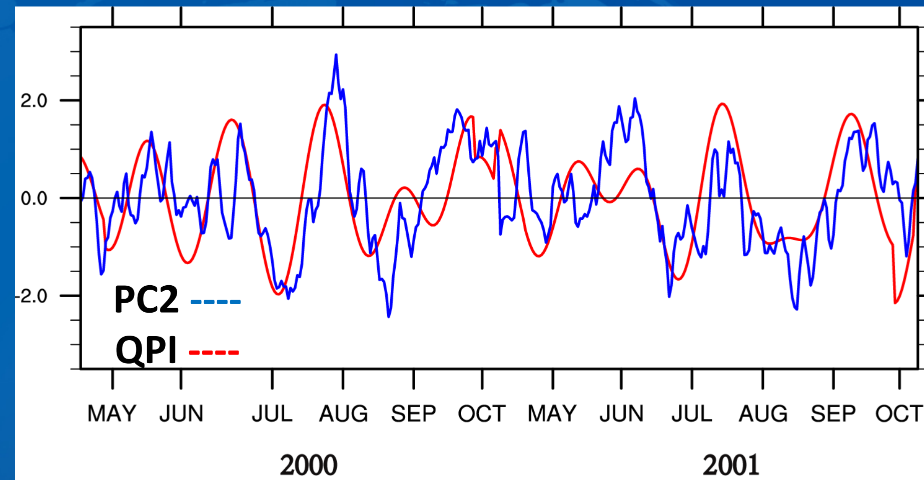

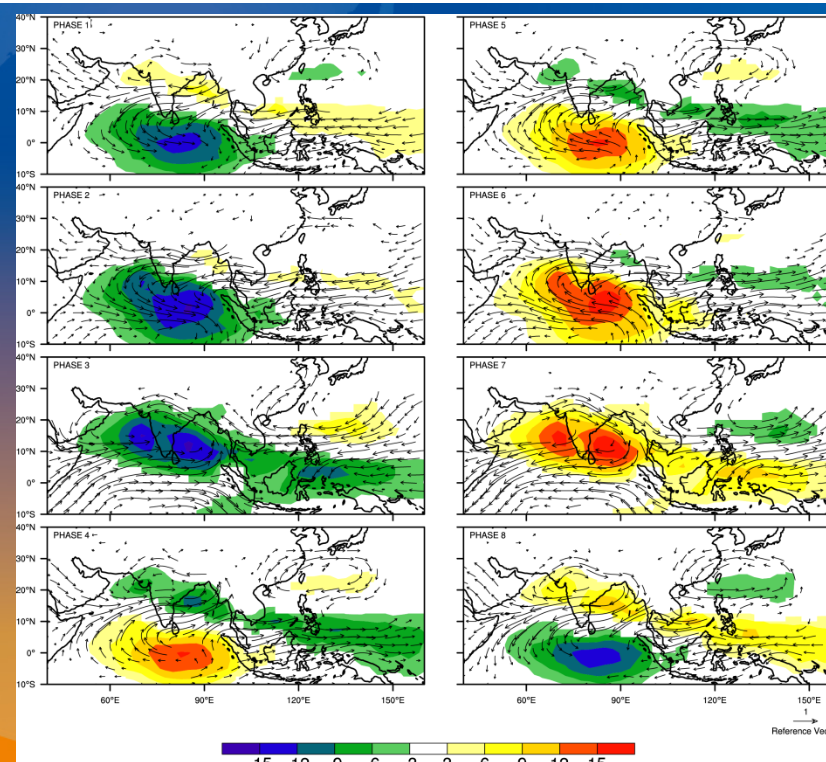

$$SADI(t) = A(t+nlag_{AB}) - B(t)$$
$$EADI(t) = C(t+nlag_{CD}) - D(t)$$
$$QPI(t) = SADI(t+nlag) - EADI(t)$$

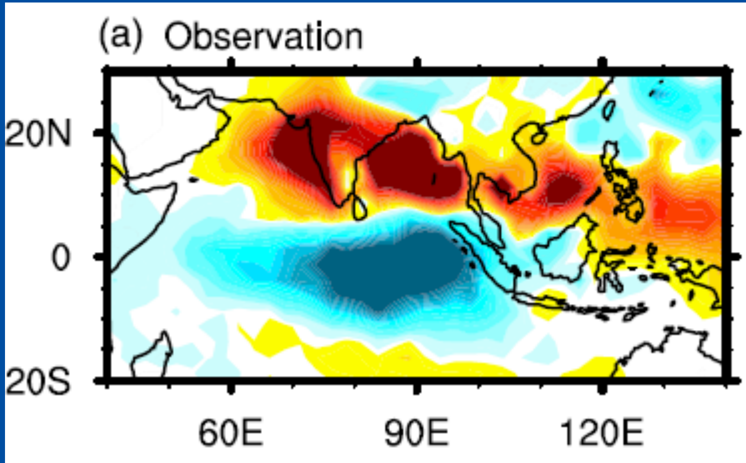

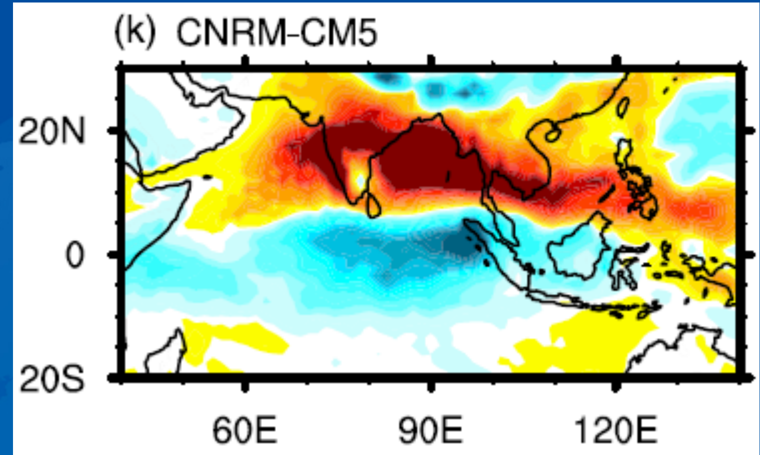

Sabeerali et al. 2013)

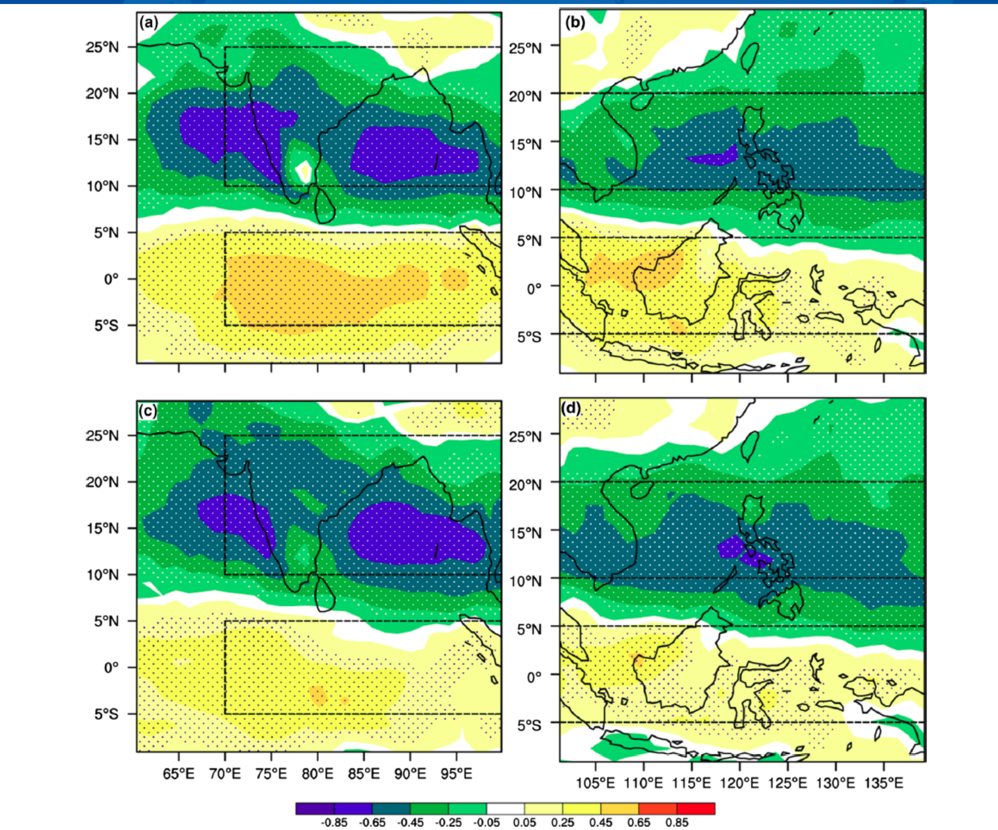

Fig. 9 Regression coefficients (*shading*) of rainfall anomalies against **a** the SADI and **b** the EADI during the boreal summer (1 May to 31 October) from the twentieth-century simulations. **c**, **d** As in (**a**) and (**b**) except for the twenty-first century simulations. *Stippling* indicates the regions where the regression coefficients are statistically significant at the 5 % significance level. The *two rectangles* represent the domains over which the time series of area-averaged intraseasonal rainfall anomaly are produced to calculate the SADI and EADI

Li and Mao (2015)

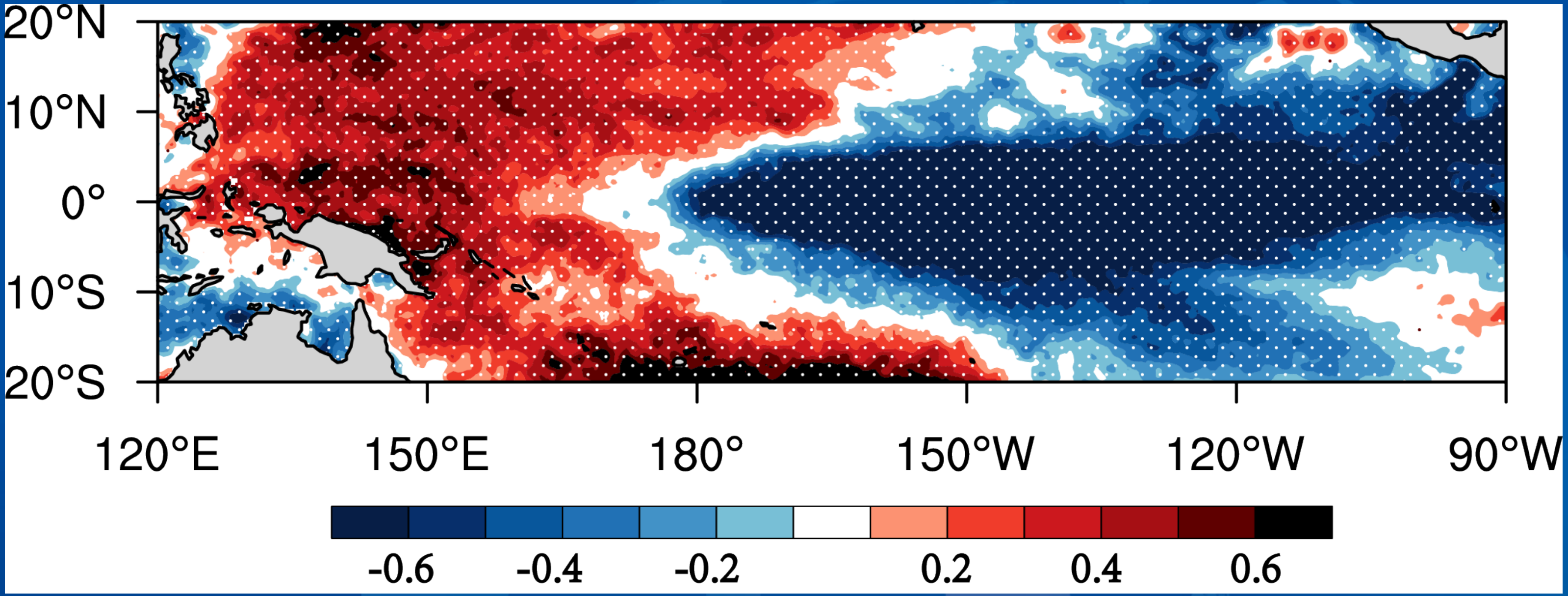

Differences between strong and weak BSISO years of seasonal-mean SST (color scale, K) over the tropical Pacific during the preceding winter (1 December–28 February). Stippling indicates the regions where the SST differences are statistically significant at the 90% confidence level. (La Nina 1996 and 2006)

For the IPCC AR5, four scenarios were designed: RCP (the representative concentration pathway) 2.6, RCP 4.5, RCP 6.0 and RCP 8.5. All of these are considered likely changes in future anthropogenic greenhouse gas emissions, with a possible range of radiative forcing in the year 2100 relative to 1850 of 2.6, 4.5, 6.0, and 8.5 W m^{-2}, respectively.

The RCP 2.6 is a mitigation scenario and the RCP 4.5 and RCP 6.0 represent stabilization scenarios, while the RCP 8.5 is a scenario of extremely high greenhouse gas emissions (IPCC 2013). The historical simulation forced by the observed atmospheric composition changes was integrated from 1850 to 2005.

The historical simulation forced by the observed atmospheric composition changes was integrated from 1850 to 2005. We extracted the simulation results over the recent 20 years from 1981 to 2000 to demonstrate present-day climate. The RCP 8.5 simulation was integrated from 2006 to 2100, and the outputs over the last 20 years from 2081 to 2100 were used to reflect future climate.

We are confident that lower-tropospheric water vapor will increase as the climate warms.

We can predict, with nearly as much confidence, that certain other changes will occur that are coupled to this increase in water apor (Hydrological response to warming).

Northward Propagating signals over South Asia

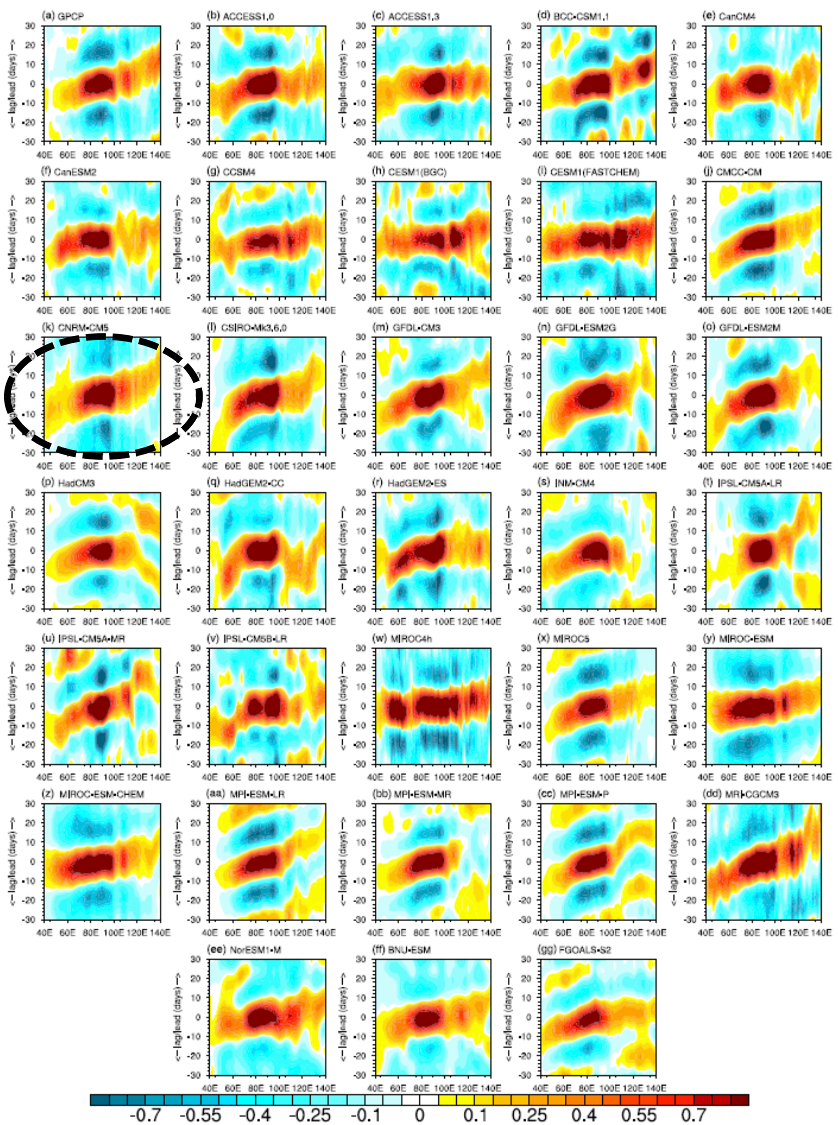

Figure 8. Lag-longitude diagrams of regressed anomalies of 20–100 day band pass filtered precipitation (mm day^{-1}) averaged between 5°S and 5°N illustrating the eastward propagation along the equatorial belt in (a) GPCP, (b–gg) 32 CMIP5 models. The 20–100 day band pass filtered precipitation anomalies averaged over 10°S–5°N and 75°E–100°E is used as a reference time series for regression.

◆ Northward Propagating Component over South Asian Sector

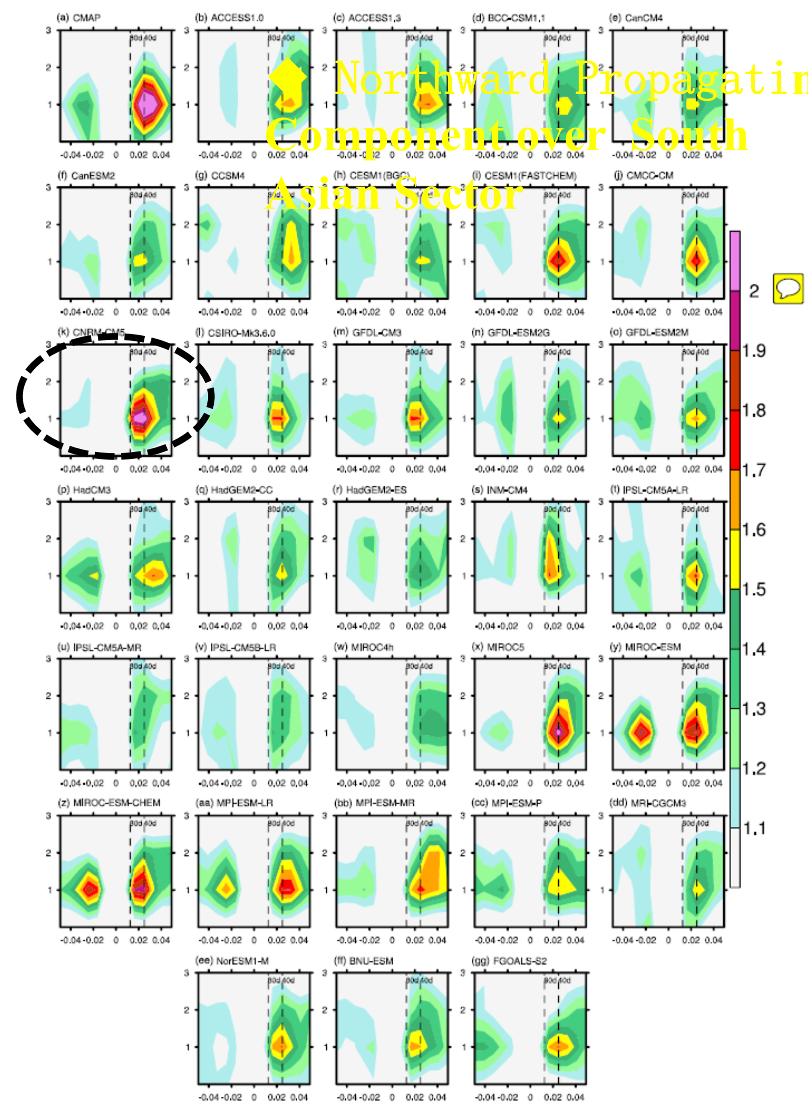

Figure 10. The finite domain space time spectra of rainfall anomalies calculated over 15°S–30°N, 60°E–100°E as a function of wave number and frequency for the northward and southward propagating BSISO (a) observations, (b–gg) 32 CMIP5 models.

Sabeerali et al. (2013)

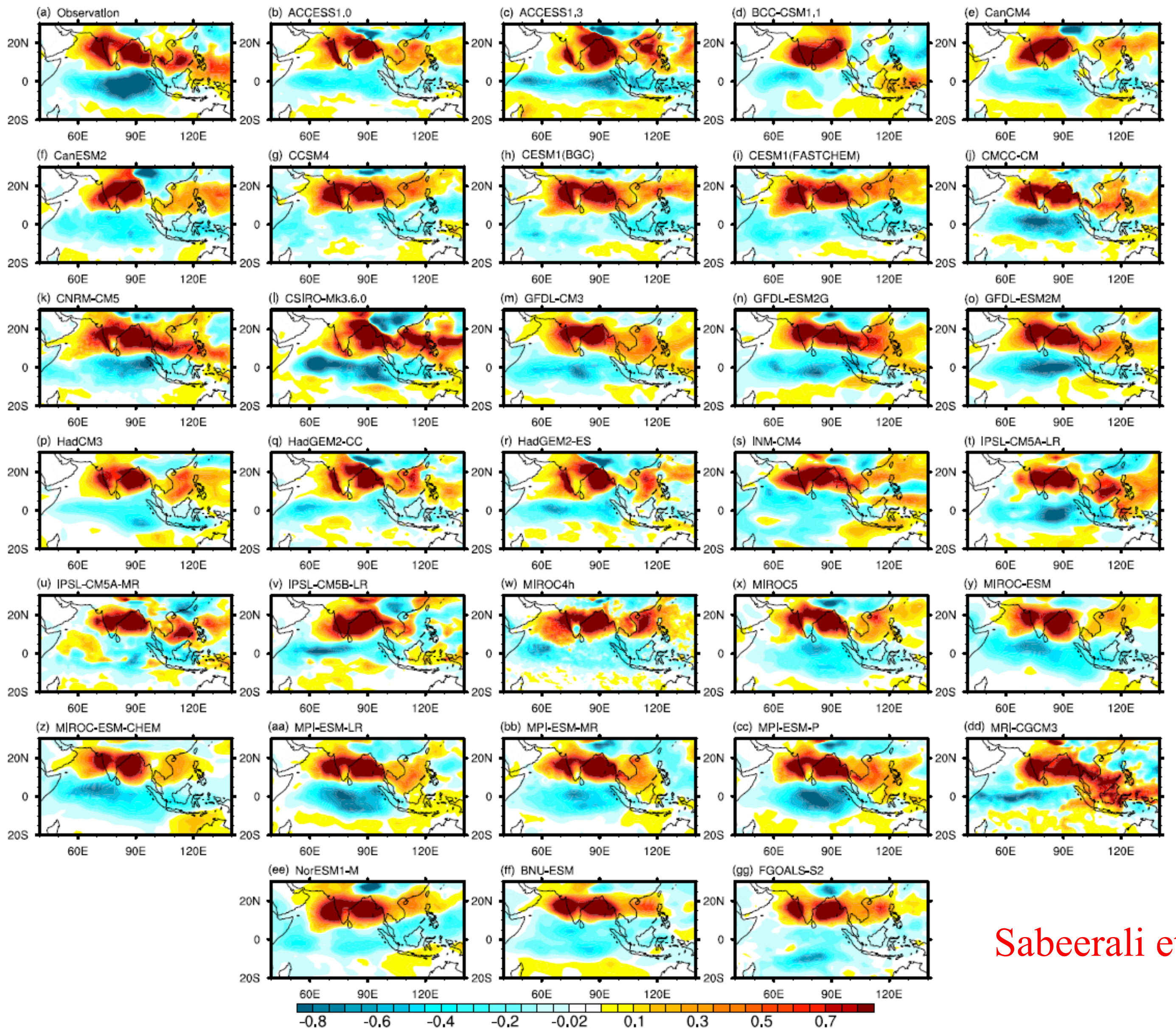

Figure 11. Regressed 20 to 100 day band pass filtered precipitation anomalies (mm day^{-1}) with reference to a reference time series created by averaging the filtered precipitation anomalies over the monsoon core region (12°N–22°N, 70°E–90°E) at zero lag (a) CMAP, (b–gg) 32 CMIP5 models.

Sabeerali et al. 2013)

1) The well simulated northward propagation of BSISO is achieved by improving the equatorial eastward propagation in the CMIP5 models.

2) By analyzing the multiple aspects of the BSISO, it is found that the models MIROC5, IPSL-CM5A-LR, GFDL-CM3, CMCC-CM, and MPI-ESM-LR represents most of the observed characteristics of the BSISO and give an opportunity to study the BSISO and its modulations under future warming scenarios (Sabeerali et al. 2013).

Although the CNRM-CM5 model reproduces the northward propagations over both the SASM and EA/WNP areas (Li and Mao 2016), the complementary relationship between these two dipoles is not well captured, with the SASM dipole being accompanied by convection anomalies with the same sign over the EWP and SCS (see fig. 11k of Sabeerali et al. 2013).